Methods to detect and characterize metal ion binding sites in RNA

Erat, M C ; Sigel, Roland K O

Abstract: Metal ions are inextricably associated with RNAs of any size and control their folding and activity to a large part. In order to understand RNA mechanisms, also the positioning, affinities and kinetics of metal ion binding must be known. Due to the spectroscopic silence and relatively fast exchange rates of the metal ions usually associated with RNAs, this task is extremely challenging and thus numerous methods have been developed and applied in the past. Here we provide an overview on the different metal ions and methods applied in RNA (bio)chemistry: The physical-chemical properties of important metal ions are presented and briefly discussed with respect to their application together with RNA. Each method ranging from spectroscopic over biochemical to computational approaches is briefly described also mentioning caveats that might occur during the experiment and/or interpretation of the results

Methods to Detect and Characterize Metal Ion Binding Sites in RNA

Michèle C. Erat[1] and Roland K. O. Sigel[2]

[1]Department of Biochemistry, University of Oxford,

South Parks Road, Oxford OX1 3QU, United Kingdom

<michele.erat@bioch.ox.ac.uk>

[2]Institute of Inorganic Chemistry, University of Zurich,

Winterthurerstrasse 190, CH-8057 Zurich, Switzerland

<roland.sigel@aci.uzh.ch>

ABSTRACT

Metal ions are inextricably associated with RNAs of any size and control their folding and activity to a large part. In order to understand RNA mechanisms, also the positioning, affinities and kinetics of metal ion binding must be known. Due to the spectroscopic silence and relatively fast exchange rates of the metal ions usually associated with RNAs, this task is extremely challenging and thus numerous methods have been developed and applied in the past. Here we provide an overview over the different metal ions and methods applied in RNA (bio)chemistry: The physical-chemical properties of important metal ions are presented and briefly discussed with respect to their application together with RNA. Each method ranging from spectroscopic over biochemical to computational approaches is briefly described also mentioning caveats that might occur during the experiment and/or interpretation of the results.

KEYWORDS

metal ions, ribozymes, RNA, methods, spectroscopy

1. INTRODUCTION

The detection of metal ions within complex RNA structures is highly challenging. Nevertheless, a profound characterization of this crucial interaction is the basis to understand folding, structure and function of any RNA, especially catalytically active ribozymes. Three major problems are to be overcome in every method that aims at investigating this relationship: (i) Only few metal ions are specifically bound, whereas most are just diffusely associated with the negatively charged phosphate-sugar backbone. The differentiation between these two groups is difficult, also because a permanent exchange takes place and RNA structures are dynamic. (ii) Metal ion binding to RNAs is by orders of magnitudes weaker than in metalloproteins thus often prohibiting a clear picture. In addition, fast ligand exchange rates and thus also varying coordination spheres over time seem to be rather the rule than the exception. (iii) The usually assumed natural cofactors Na^+, K^+, Mg^{2+}, and possibly Ca^{2+} are mostly spectroscopically silent. Hence only indirect observation or the replacement with another (spectroscopically active) ion is possible. In the latter case though one has to be aware of the introduced deviations from the wild-type system.

In this review, we try to give a comprehensive overview on the methods that have been applied in the past as well as on those that might become more important in the future to investigate and characterize metal ion-RNA (or nucleic acids in general) interactions. Obviously it is impossible to cover every method to the same extent, and hence we will concentrate in more detail on those that we have applied ourselves in the past, whereas others shall be discussed rather briefly and the reader will be referred to the corresponding literature. One aim of this review is not only to highlight the advantages and results, but also to list the caveats and possible difficulties associated with of each method. In this sense, many of the aspects discussed in more detail in the context of one method are directly applicable to others.

2. GENERAL CONSIDERATIONS

2.1. Metal Ions to be Considered for RNA Binding

Neither RNA nor DNA can exist without cations compensating for their accumulated negative charge of the phosphate sugar backbone at physiological pH. In principle, also organic cations, e.g., polyamines, can be used for this purpose but in reality monovalent and divalent metal ions will

carry the major burden of charge compensation. For life in general, numerous metal ions are essential and are thus found in living cells in a large range of concentrations, which are tightly regulated (Figure 1). However, most of these metal ions are strongly bound within metalloproteins and are thus not freely available. In fact, only Na^+, K^+, Mg^{2+}, and Ca^{2+} are available in their solvated form in larger amounts. Nevertheless, Na^+ is primarily found outside the cell compartment and millimolar Ca^{2+} concentrations are found only in specialized compartments/cells acting as a neurotransmitters. Consequently, K^+ and Mg^{2+} are usually considered the natural metal ion cofactors for nucleic acids *in vivo*.

This view might actually be oversimplified. For example, two different hammerhead ribozymes were examined towards their catalytic activity in the presence of various divalent metal ions [1,2]. In both cases, strong increases in cleavage rate were observed when substituting Mg^{2+} with a transition metal ion, e.g., a 400 times accelerated catalysis of the RzB *Hammerhead* in the presence of Mn^{2+} [2]. However, this change in activity does not hint *per se* towards the usage of other metal ions in nature but just exemplifies that the metal ion-RNA interaction and the basic coordination properties of each metal ion are the key co-factor for RNA structure and activity. The increase in activity of the *Hammerhead* ribozyme in the presence of transition metal ions thereby does not follow the Irving-Williams series, but rather the intrinsic affinities of the metal ions towards phosphate groups [3] (Figure 2 and Table 1). Consequently, the extent of the thermodynamic interaction of the divalent metal ion with the bridging phosphate groups (possibly even the cleavable phosphodiester) is the determining factor for cleavage activity of this small ribozyme. This notion is supported by the fact that the phosphate groups are the major primary binding sites for most metal ions [4,5], whereas further interactions incrementally increase the overall affinity [5].

The situation immediately becomes more complicated in cases where the change in catalytic activity deviates from such basic metal ion properties (Table 1). For example, a ribozyme derived from the yeast mitochondrial group II intron Sc.ai5γ is strongly inhibited in the presence of small amounts of Ca^{2+} [6] (see also Chapter 7). By single molecule FRET studies it has been shown that this inhibition possibly results from the formation of a misfolded species [7]. As the phosphate affinity of Mg^{2+} is larger only by a factor of about 1.3 (see also Section 2.2), but Ca^{2+} already strongly inhibits at a 20-fold excess of Mg^{2+}, this means that specific binding pockets for Ca^{2+} must

exist, possibly resulting in a cooperative accumulation of Ca^{2+} within the misfolded RNA. Considering that Ca^{2+} in mitochondria can reach millimolar levels and thus almost equal Mg^{2+} concentrations, a biological role of the Mg^{2+}/Ca^{2+} switch is well feasible, although possible roles of metal ions other than Mg^{2+} *in vivo* remain largely unexplored in the context of ribozymes.

In contrast to this obvious lack in knowledge of the situation *in vivo*, such experiments with various metal ions to elucidate structural and functional aspects of metal ions in nucleic acids are commonly performed *in vitro*. The specific chemical and physical properties of specific metal ions are thereby used to investigate for example catalytic mechanisms as described in the following section.

2.2. Chemical and Physical Properties of Commonly Used Metal Ions

Aside from Mg^{2+} a multitude of different metal ions is applied in combination with nucleic acids in daily research experiments (Figure 1). These can be either divalent ions (Table 1) or for many purposes also members of the Lanthanide series (Table 2). Especially for X-ray crystallography, a large part of the Periodic Table of metal ions has been explored, as is obvious from the deposited structures in the PDB (Protein Database) (Figure 1). One thereby takes advantage of the better diffracting properties of heavier metal ions (see also Section 3.1.3), often enabling to solve the phase problem by Patterson methods. Other common examples where different metal ions are employed, include thio-rescue and related experiments (see Sections 4.1 and 4.2), hydrolytic and oxidative cleavage experiments (see Sections 4.3 and 4.4) to probe metal ion binding sites or even specific liganding atoms on the nucleic acid.

Often, also the intrinsic properties of the (solvated) metal ion itself are used: The correlation of the pK_a of coordinated water molecules with the pH profile of the reaction allows conclusions on the (metal ion assisted) acid-base mechanism of catalysis [2]. EPR active metal ions can be applied to investigate directly the coordination sphere or elucidate the number of tightly bound ions in a folded RNA (see also Section 3.3). Lanthanide ions have interesting spectroscopic properties allowing conclusions on their binding (see Section 3.4), and NMR active nuclei also allow a view on the metal ion itself (see Section 3.2.3).

Some chemical and physical properties of often applied divalent and Lanthanide metal ions are summarized in Tables 1 and 2. The comparison of these accumulated data immediately

illustrates that there are clearly two sides to the coin. On the one hand, the usage of different metal ions provides the opportunity to observe the metal ion directly, shift the acid base profile of catalysis, or selectively probe a coordination site, thus yielding crucial information on the metal ion binding. On the other side, no two metal ions will behave identically, and thus results obtained with metal ions other than the natural cofactor will always be burdened with the caveat that one cannot be sure if the system applied is meaningful. Nicely illustrated is this fact by crystal structures of identical RNAs, but containing different metal ions, which often don't occupy identical positions (see also Section 3.1). Nevertheless, if one is aware of the specific coordinating properties each metal ion, the advantages and opportunities of varying the kind of metal ion are clearly manifold.

2.3. Prerequisits to the RNA and the Experimental Conditions

For all the methods described in this review, the RNA should be as uniform as possible. The RNA sequences, depending on their length and possible modifications, can be obtained by chemical synthesis [8,9] or transcription by T7 RNA polymerase. Transcription and purification of RNA to obtain a uniform sample has been described before [10-12]. To quantify metal ion binding to RNA under situations where the metal ion is not in large excess, it is crucial to be aware that the 5'-end of the transcribed RNA carries a triphosphate chain. This site is likely to be the primary binding site for metal ions [13] and thus needs to be accounted for , if it is not removed by kinases [12].

Further factors can influence the metal ion affinity considerably: Both, ionic strengths [14] and solvent polarity [15-18] are well known factors. In addition, it is important to use buffers that are not good ligands for metal ions at the same time. For example, citrate, phosphate, or the very commonly used Tris-HCl bind metal ions rather well [19]. As most buffer substances are applied in much higher concentration than the metal ion itself, these ligands can interfere with binding of metal ions to nucleic acids [20,21].

3. SPECTROSCOPIC METHODS

3.1. X-ray Crystallography

X-ray crystallography is a magnificent method to obtain insight into structural relationships between RNA and its coordinating metal ions. As of May 2010, 21799 Mg^{2+} ions bound to RNA are deposited in the PDB that have been identified by X-ray crystallography. If the resolution is

sufficient, the bound alkaline and earth alkaline metal ions can be directly observed. However, more commonly, metal ion binding sites are obtained by soaking a crystal with solutions of heavier metal ions to identify binding sites. The following section gives a brief overview of the major advantages and pitfalls of the method and describes a few examples, where X-ray crystallography has been useful in deciphering metal ion binding sites in RNA.

3.1.1. Setup of RNA Crystal Screens

Prior to setting up crystallization screens, the concentrated RNA needs to be refolded into its native state. The RNA is heated to 90°C for a few minutes and left to cool slowly to room temperature. To avoid self cleavage of the RNA, it is advisable to keep the pH slightly acidic and to add divalent cations only around 35 °C [11].

Once the sample is ready, one can proceed to setting up crystallization screens. The main crystallization method used in macromolecular crystallography today is the vapor diffusion technique in a hanging or sitting drop setup. Crystallization is initiated by concentrating the RNA containing droplet against a comparatively large volume of reservoir solution. Crystallization robots enable the screening of many thousands conditions in a relatively short time. For initial broad screens, specific crystallization sparse matrices have been developed and many of them are commercially available, e.g. from Hampton Research, Emerald Biosystems or Qiagen. General considerations for crystallization of nucleic acids are similar to those for protein crystallization, but it has been noted that higher temperatures (37 °C) seem to favor RNA crystal formation [11]. Further factors that can be varied in order to find the optimal crystallization conditions include buffer, pH, precipitant and salt identity and concentration (Figure 3). Although RNA is less sensitive to small pH changes than proteins, this factor should not be entirely discarded, as tertiary contacts in larger RNAs can shift the pK_a of titratable groups closer to neutrality [22].

If no crystals appear in any of the conditions tried, it may be worthwhile to consider a change in construct. Sometimes minor variations in length or sequence can result in a shape that has a higher propensity to pack in a regular manner. Once a first hit has been obtained, the long process of optimization starts. The following rules of thumb might be useful when analyzing initial results: Precipitates usually call for a decrease in RNA and/or precipitant concentration. Note, that microcrystals can be mistaken for small precipitates. It is therefore advisable to carefully inspect

those conditions under the microscope. If microcrystals or clusters of homogenous crystals are found, it can be helpful to slow down the diffusion process by either lowering the temperature, or covering the reservoir solution with oil. If phase separation is a problem, the monovalent salt concentration can be increased and/or the precipitant concentration lowered. If the droplets remain clear, it may be that the construct has a low propensity to crystallize (see above). Alternatively the RNA concentration simply may lie outside the nucleation zone (Figure 3), in which case a repetition of the screen with higher RNA and/or salt concentrations may solve the problem. At the end of the day, macromolecular crystallography remains to some extent a "black art"; but the more conditions are tried, the higher the probability of success. A helpful link in this respect is provided by Hampton Research (http://hamptonresearch.com/tips.aspx).

3.1.2. Direct Observation

Due to the equal number of electrons of Na^+, Mg^{2+}, and a water molecule, it is difficult to unambiguously distinguish the three. This problem as well as strategies to solve it have been excellently described and reviewed before [23,24]. Most importantly a high enough resolution is crucial to directly observe metal ions in crystal structures. One of the most prominent examples is the structure of the large ribosomal subunit of *Haloarcula marismortui*, in which 116 Mg^{2+} and 88 M^+ ions have been unambiguously positioned [25]. This was done by an iterative method: First, a list of candidates was generated in an automated fashion by searching $F_{obs} - F_{calc}$ difference electron density maps for peaks that were 1.9–2.1 Å from ribosomal nitrogen or oxygen atoms. If the surrounding electron density features agreed with an octahedral conformation, these electron density peaks were modeled as Mg^{2+} (Figure 4). The modeling of the first hydration shell was also based on $F_{obs} - F_{calc}$ difference maps. The identity of the complex was confirmed if a refined distance of 2 Å between Mg^{2+} and H_2O was found. At last, fully hydrated Mg^{2+}_{aq} ions were identified by visual analysis of the electron density maps.

3.1.3. Identification of Metal Ions by Heavy Metal Soaking

For lower resolution structures, metal ion binding sites can potentially be identified by soaking the crystals in solutions of heavier metals, such as Tl^+, Rb^+, Mn^{2+}, Pb^{2+}, Co^{3+}, Os^{3+}, Eu^{3+}, or Ir^{3+} [26]. This method has already been applied to identify metal ions in the first crystal structure of

the hammerhead ribozyme in 1994 [27]. Traditionally this strategy is used to solve the phase problem by Patterson methods. As outlined above in Section 2.2, metal ions are very distinct with respect to their binding properties. It is thus important to use metal ions that are as similar in their chemical and structural features as possible to the ion that is suspected to bind under native conditions, i.e. mostly Mg^{2+}. If possible, it is useful to validate the analogous behavior of the light and heavy metal ions by biochemical methods. Unfortunately this approach is not always successful. In case of the large ribosomal subunit for example, replacement of $MgCl_2$ by $MnCl_2$ invariably caused crystal twinning [25].

An interesting application of heavy metal soaking of RNA crystals was reported by Wedekind and McKay [28], in a study of metal ion binding sites in the leadzyme. This small ribozyme, that has been discovered through *in vitro* selection [29,30], depends on Pb^{2+} for activity [31,32] (see also Chapter 4.3.2). It can be inhibited by addition of Mg^{2+} whereas ions that displace Mg^{2+} restore activity. Because of the disorder induced by cleavage at the scissile phosphate bond in presence of Pb^{2+}, it is not possible to determine the exact differences between Mg^{2+} (ground state) and Pb^{2+} (catalytic state) binding by soaking the leadzyme extensively with Pb^{2+} salts. Here, instead of Pb^{2+}, Sr^{2+} was used, which has a similar ionic radius and mimics Pb^{2+} in binding, but not in catalysis. After crystallization, the crystals were soaked with either Mg^{2+} only or Mg^{2+} and Sr^{2+}. The metal soaked samples were flash-frozen and data were collected to a resolution of 1.8 Å, at which the coordination geometry of the metal ions could be observed directly. Sr^{2+} ions were identified in difference Fourier maps. On the basis of this experiment, the participation of a metal ion binding to a remote site as a catalytic regulator of the leadzyme was deciphered.

3.1.4. Time Resolved Crystallography

If homologous structural intermediates exist that can be either rapidly visualized or trapped, time resolved crystallography allows the direct observation of structural changes that occur during the reaction. Trapping of intermediates is achieved by either adjusting a controlling variable (pH, metal ion concentration, etc.) or by flash freezing the crystal. Scott et al [33] captured a structure of the hammerhead ribozyme in the ground state with bound metal ions by lowering the pH < 5.0 and subsequent flash freezing. In a second experiment, Mg^{2+} was allowed to induce cleavage at pH 8.5 prior to flash freezing. In this way, conformational rearrangements of the ribozyme to reach the

active transition state could be elucidated.

Time resolved crystallography is a very elegant method to decipher differences in metal ion coordination between the ground – and an intermediate state. In general, it is of course possible, that the trapped conformations would not significantly accumulate in solution and further biochemical experiments are necessary to verify the reaction pathway proposed by this technique.

3.1.5. *Limitations*

Crystal structures will only provide snapshots at a specific point in time under strictly controlled conditions that may not necessarily coincide with the most highly populated conformation in solution [26]. Especially for ribozymes it is important to know that in order to capture enzyme-substrate complexes, one needs to perturb the active site or a parameter that is important for activity (see time resolved crystallography), which may lead to a change in metal ion positioning [34].

Due to the equal number of electrons in Na^+, Mg^{2+} and H_2O, these ions can only be distinguished on the basis of geometric criteria requiring high resolution data [35]. To unambiguously identify a particular metal ion, it may be necessary to carefully analyze the anomalous signal or solve the structure in presence of heavier metal ions that prefer a similar coordination environment [24]. However, Ennifar et al. [36] have shown in a detailed crystallographic study of two HIV-1 dimerisation initiation site RNA duplexes containing various different metal ions, that Mg^{2+} containing crystals were not isomorphic to crystals with other ions and that no two kind of ions bind identically to the RNA [3,4,36], as is also illustrated in Figure 4b. This is clear evidence that different ions may stabilize slightly different RNA conformations and care needs to be taken when extrapolating results obtained with one ion to another.

In summary, crystal structures, albeit a great tool to gain insight into the coordination of metal ions to nucleic acids, need to be treated with a healthy skepticism. If structures from the PDB database are used to interpret results of biochemical or spectroscopic experiment, it is essential to have a close look at the experimental data and the conditions used for crystallization.

3.2. NMR

Besides X-ray crystallography, nuclear magnetic resonance (NMR) has become the second power horse for the determination of biomolecular structures at atomic resolution. NMR is

particularly suited to study interactions between biomolecules and their ligands in solution. Especially for nucleic acids, NMR has often proven the method of choice. 42.4 % of all nucleic acid structures deposited in the PDB database by June 2010 were solved by NMR. And because metal ions are always intricately involved in RNA folding, it comes as no surprise that already the first ribozyme structure to be determined in its entirety by NMR revealed details about the importance of metal ion binding [37].

Naturally abundant isotopes in nucleic acids that are suitable for detection by NMR are ^{1}H and ^{31}P. Furthermore, it has become standard practice to produce isotopically enriched RNA by *in vitro* transcription with commercially available ^{13}C,^{15}N-NTPs [10].

NMR is a very powerful method for the observation of metal ion induced changes of RNA structure in solution. Metal ion binding alters the chemical shifts of nearby NMR active nuclei. These chemical shift changes can be plotted against the metal ion concentration and fitted to a 1:1 binding model, to calculate affinity constants [38,39] (see also Section 6). The diamagnetic Mg^{2+} ion, that is the most common divalent ion to bind nucleic acids *in vivo*, is well suited for this purpose. It is important to note, that chemical shift changes only report the change in the electronic environment of the observed nucleus, which can be caused by the electron withdrawing effect of the metal ion binding nearby or by structural changes in the local geometry and/or the global fold of the molecule. Chemical shift maps alone do not give any information as to what exactly caused the observed change, and thus have to be interpreted with caution. Fortunately, NMR itself lends a hand in finding alternative ways for the detection of metal ion binding sites.

In the following section, we try to outline the most commonly used NMR methods for the detection and characterization of metal ion binding sites in RNA.

3.2.1. 1D-NMR Methods

3.2.1.1. [^{1}H]-NMR

The quickest way to detect interaction of metal ions with RNA by NMR is to record simple [^{1}H]-spectra and observe changes in the imino proton resonances of uracil NH_3 and guanine NH1 upon addition of increasing amounts of metal ions (Figure 5). This approach does not require any labeling of the RNA and is sensitive enough to be carried out with relatively low concentrations of the nucleic acid (minimum 0.2 mM). It is thus often used to screen for optimal experimental

conditions. Because the imino protons can exchange with the protons of the solvent, these experiments are recorded in 90% H_2O / 10% D_2O and water suppression is essential to obtain valuable spectra. Furthermore low temperatures slow the exchange with the solvent. However, we observed surprisingly sharp signals at 293 K [40]. Considering the general line-broadening effect due to slower molecular tumbling at low temperatures, it may not only be unnecessary, but detrimental to cool the sample too much.

Depending on the metal ion and whether an interaction with the RNA is taking place, changes in chemical shift or line width broadening is observed upon metal ion addition. Whereas paramagnetic ions, such as Mn^{2+}, induce broader lines in a distance dependent fashion [41], the diamagnetic Mg^{2+} ion is commonly used to observe chemical shift changes. Unfortunately the exchange rate with Mg^{2+} often falls in the µs – ms range, corresponding to an intermediate exchange on the NMR timescale, thus also leading to line broadening [42,43] (see also Section 3.2.2.1). Although this is commonly regarded as a drawback of the method, it can be used to verify the significance of the observed chemical shift changes: If the proton resonances that experience the largest chemical shift change also broaden during the titration, this implies that the observed chemical shift changes are due to a direct effect of the metal ion and not due to long range structural changes.

However, imino protons are usually located far away from the metal ion coordination site and their chemical shift is additionally dependent on the local structure and the exchange rate with the solvent [38]. Even more importantly, adenine and cytosine moieties cannot be observed and metal ion binding to bulge regions can often not be followed, as such imino protons become broadened beyond detection due to the exchange with the solvent [38]. Thus, observing changes in the imino proton resonances in [^{1}H]-NMR spectra is solely a quick and easy way to determine, whether a metal ion has any influence on the studied RNA. However, it is a highly insufficient and also misleading method to yield any more details on the M^{n+}-RNA interaction. Hence, once an interaction is detected, it is advisable to use one or several of the methods described below to gain more insight.

3.2.1.2. [^{31}P]-NMR

The phosphate group that links sequential nucleotides is negatively charged and thus presents

a primary cation binding site in RNA [3-5,44-46]. [^{31}P]-NMR seems the obvious choice to detect metal ion-phosphate oxygen interactions in nucleic acids: Already in 1999, Pardi and coworkers [47] have identified a novel metal ion binding site in the hammerhead ribozyme by [^{31}P]-NMR. They were able to observe a single resonance that broadened before any other resolved resonance upon addition of the paramagnetic Mn^{2+}. This resonance was assigned by the incorporation of a non-bridging ^{17}O using enriched H$_2$^{17}O, because ^{17}O efficiently broadens the attached ^{31}P by quadrupolar relaxation [48].

Unfortunately, apart from the 5'-end of a nucleic acid chain and some very special cases, most resonances are ill resolved in the ^{31}P spectrum, clustering around 0 ppm (Figure 6). One way to overcome this problem is to exchange a non-bridging phosphate oxygen at the position of interest with sulfur. Phosphorothioates are shifted far downfield to around 60 ppm in the ^{31}P NMR (Figure 6). Potential interactions with thiophilic metal ions, such as Cd^{2+}, can then be followed by observation of chemical shift changes of these well resolved residues [49-51]. Care has to be taken when interpreting these data: Large downfield shifts upon addition of M^{n+} ions do not necessarily mean a direct coordination [52], as it was erroneously claimed in studies with nucleoside 5'-triphosphates and 5'-diphosphates in the 1970s [53,54].

The two non-bridging phosphate oxygens are pro-chiral, i.e. the R_P phosphate oxygen points towards the major and the S_P towards the minor groove. The R_P oxygens can be replaced easily and stereoselectively, using α-thio NTPs in the *in vitro* transcription reaction: T7 RNA polymerase only incorporates S$_P$-α-thio-NTPs in an S$_N$2 type reaction by inversion of configuration without effect on the transcription yield (see also Section 4.1.1). Naturally, *in vitro* transcription will introduce a phosphorothioate 5' of each nucleotide class that has been added in the form of α-thio-NTP. For the site-specific incorporation of phosphorothioates, solid phase RNA synthesis is the only option. Unfortunately solid phase synthesis cannot distinguish between R_P and S_P phosphorothioate introduction and therefore this approach will always lead to a mixture of stereoisomers. Although separation of the two isomers should technically be achievable by HPLC [55], we did not succeed with a 27mer oligonucleotide [56]. Nonetheless, such site specifically incorporated phosphorothioates can be useful to help resonance assignments.

The replacement of a phosphate by a thiophosphate group is not necessarily an innocent mutation [57]. Hence, it needs to be checked whether the incorporation of sulfur has an effect on the

stability of the RNA, e.g., by UV melting curves. In addition, [^{1}H,^{1}H]-NOESY and [^{1}H,^{13}C]-HSQC fingerprint spectra can indicate structural differences by changes in the chemical shift pattern between wildtype and thioated RNA.

3.2.1.3. [^{15}N]-NMR

Another 1D method that has been put forward mainly by Tanaka and Taira [58,59], is the use of direct [^{15}N]-NMR spectroscopy to probe metal ion binding to nucleobase nitrogen atoms. For this approach, the RNA needs to be isotopically enriched with ^{15}N (spin ½). This can be achieved by using ^{15}N-enriched NTPs in the *in vitro* transcription reaction. Tanaka et al identified a metal ion binding site on an RNA motif derived from the hammerhead ribozyme [58] and analyzed its binding properties in detail [59].

In contrast to [^{1}H]-NMR, [^{15}N]-NMR provides a tool to directly observe a coordinating atom. Tanaka and Ono have investigated the effect of Hg^{2+} coordination to a DNA duplex in detail and conclude that innersphere coordination is accompanied by an upfield shift of the affected ^{15}N resonances, whereas proton – metal cation exchange leads to a downfield shift [60]. In the case of an imidazole modified DNA duplex, Ag$^+$ coordination caused an upfield shift of the liganding N3 by almost 20 ppm [61]. Again, broadening of the line width can be an issue, if the exchange regime proves unfavourable [58].

The same authors have also tried to directly detect metal ion binding through 1-bond ^1J couplings between the metal ion and the nucleobase ^{15}N in 1D ^{15}N NMR spectra, as it has been done for metalloproteins [62,63]. To our knowledge this approach has not been successful so far, probably due to exchange processes between the metal bound and the metal free states of the RNA [58-60].

At least in theory, ^{15}N NMR is an ideal method to probe the direct interaction between a metal cation and a nucleobase nitrogen in solution, because the ^{15}N chemical shift is very sensitive to changes in the local environment [64]. For example, a 20 ppm upfield shift has been measured for the N7 of guanosine in DMSO upon addition of one equivalent of Zn^{2+} or Hg^{2+} and the protonation of an adenosine N1 causes a 70 ppm upfield shift [65,66]. Unfortunately, the low gyromagnetic ratio of nitrogen leads to a rather low signal of directly observed ^{15}N nuclei, and thus, extensive recording times (10 – 20 h) are needed to obtain a simple 1D spectrum. Also spectral assignments

of larger RNAs are complicated. To overcome these issues, it may in fact be easier to record 2D proton-nitrogen correlated HSQCs as described below, to probe direct interactions between metal ions and nucleobase nitrogens.

Using indirect detection in an HSQC type experiment, Johannsen et al. measured a 86 Hz splitting of the N3 resonances of three consecutive ^{15}N labeled imidazole moieties in a palindromic modified duplex DNA structure, coordinating three Ag(I) ions [61]. This splitting was interpreted as corresponding to the average coupling of $^1J(^{15}N, ^{107}Ag)$ and $^1J(^{15}N, ^{109}Ag)$, as both silver isotopes have an almost identical natural abundance. The observed coupling constant reports directly on the coordination of Ag(I) to the N3 position of the imidazole moieties and represents the largest of this type published to date [67,68].

3.2.2. 2D-NMR methods

Although a wealth of information can already be obtained by analysis of 1D NMR spectra, there are limits, which can by overcome by applying multidimensional spectra: First and foremost, the spectral overlap is significantly reduced and often spectral assignment of any RNA would not be possible otherwise. Also, by recording heteronuclear experiments, chemical shift changes affecting multiple nuclei can be traced simultaneously. And last but not least, insensitive nuclei, such as ^{15}N (see also Section 3.2.1.3) can be probed indirectly via heteronuclear quantum coherence experiments, with the signal intensity of the much more sensitive, directly attached protons. The diversity of multidimensional NMR experiments for the assignment of peaks and thus structure determination of nucleic acids is enormous: Many of them could in theory be used to analyze the effect of metal ion binding to RNA. This section does not aspire to be complete in any way, but we want to outline the most commonly used methods, their advantages and their drawbacks and hopefully inspire scientists to try one or the other in their own facilities.

3.2.2.1. Chemical Shift Change Analysis with Diamagnetic Metal Ions

The caveats of using exchangeable protons to detect metal ion binding have been indicated in Section 3.2.1.1. Much more sensible is thus the observation of non-exchangeable protons. The classic experiment for resonance assignment of protons in nucleic acids, the $[^1H,^1H]$-NOESY [69] can also be used to monitor the effects of M^{n+} coordination to RNA at both the sugar and the nucleobase moieties. These observed protons, e.g. the H8, H2, H6, H5 and H1', are located close to

potential binding sites, such as N7 of purines, carbonyl oxygens atoms of guanines, cytosines and uracils, or 2'-OH of the ribose sugar. Chemical shift changes that are observed during titration of increasing amounts of $MgCl_2$ can be fitted to a 1:1 binding model to calculate affinity constants [38,39] (for a more detailed description thereof, see also Section 6). These chemical shift changes occur either due to direct metal ion binding or because of structural changes induced by coordination of the metal nearby, i.e. increased or reduced stacking interactions. From the information content of the chemical shift data alone, it is impossible to distinguish between these two effects. As described above, Mg^{2+} addition can lead to a substantial line broadening of some RNA proton resonances, an effect that has been allocated to an intermediate exchange of the Mg^{2+}_{aq} ion at its binding site on the NMR time scale [42,43]. The line broadening can thus be used to detect specific Mg^{2+} sites, as it should only be observed at sites, where Mg^{2+} binds in close proximity. By including this information into the evaluation, an accurate picture of metal ion binding can be obtained. Indeed in the study of metal ion binding to the shortened domain 6 of the group II intron *Sc*.ai5γ (D6-27), resonances that experienced line-broadening were the same or close in space to resonances that experienced a large chemical shift change upon the addition of Mg^{2+} [13].

The exchange phenomena observed with Mg^{2+} become severe above a concentration of about 10 mM, impairing further chemical shift analyses. Especially for weak binding sites that are not approaching saturation at this metal ion concentration, it would therefore be useful to have an alternative metal ion at hand that mimics Mg^{2+} binding, but has a faster solvent exchange kinetic than Mg^{2+}. Metal ions with this property include Cd^{2+}, which exhibits a markedly faster solvent exchange rate ($4x10^8$ vs $5.3 x10^5$ s^{-1}, see also Section 2.2). In our studies with *Sc*.ai5γ D6-27, we have titrated the RNA with Cd^{2+} and observed the chemical shift changes of the RNA proton resonances in the $[^1H,^1H]$-NOESY [40]. Like Mg^{2+}, Cd^{2+} preferentially forms non-distorted octahedral complexes. Although Cd^{2+} has a larger ionic radius than Mg^{2+} (0.97 vs 0.72 Å), it has been widely applied to mimic Mg^{2+} in biochemical studies [50,51,70-72]. Furthermore, Cd^{2+} selectively replaces Mg^{2+} bound to N7 via an innersphere coordination mode [4,36]. In our studies, Cd^{2+} concentrations above 10 mM led to increased line width, suggesting that even with cadmium(II), the exchange regime was not entirely on the fast NMR timescale. But compared to Mg^{2+}, saturation was reached in most cases, indicated by the ceased move of chemical shifts. In general, Cd^{2+} thus binds with a slightly higher affinity to the RNA than Mg^{2+}, and insofar Cd^{2+}

titrations proofed useful to elucidate weaker binding sites. In the light of the inherent ambiguity concerning the physical origin of a particular chemical shift change, it may be revealing to compare the chemical shift pattern obtained from titrations with different metal ions.

3.2.2.2. *Line Broadening Analysis Using Paramagnetic Metal Ions*

The paramagnetic Mn^{2+} has widely been used to probe for the spatial proximity of an RNA residue to the metal ion [73-75]. Line broadening is caused by distance-dependent $(1/r^6)$ relaxation of NMR active nuclei near the binding site of the paramagnetic metal ion [41]. Therefore, Mn^{2+} broadening studies can be used to distinguish residues that bind directly to divalent metal ions from residues that exhibit a structural change upon metal ion binding. For example, in a group II Intron branch domain D6-27 the crosspeaks associated with the GU wobble pairs flanking the branch-adenosine A20 became distinctly broadened upon addition of Mn^{2+} [13]. In contrast, the branch adenosine H1'-H8 and H1'-H2 as well as the interstrand A20H2-G8H1' crosspeaks were hardly affected, indicating that rather the flanking GU wobble pairs than A20 N7 are involved in binding of a divalent metal ion. Line broadening is observed already at micromolar metal ion concentration, whereas millimolar concentrations of Mg^{2+} are needed to induce chemical shift changes. If the Mn^{2+} concentration exceeds 10-20% of a 1 mM RNA concentration, non-selective broadening of all peaks in parallel has been observed for D6-27.

3.2.2.3. *Cobalthexammine as Probe for Outer Sphere Interactions*

When talking of Mg^{2+} binding sites in RNA, a question that commonly occurs is, whether the coordination mode is inner-sphere, e.g. the metal ion is in direct contact with the RNA, or outer-sphere, in which case the interaction is mediated by water molecules. Because of their similar geometry $[Co(NH_3)_6]^{3+}$ is commonly used as a probe for binding sites of fully solvated magnesium ions $[Mg(H_2O)_6]^{2+}$ [76-79]. If the cobalt(III)hexammine is in fast exchange between the bound and unbound state, a single resonance at 3.65 ppm represents all 18 ammine protons [77]. Fortunately, no protons from the RNA resonate in this region and therefore NOEs between the $[Co(NH_3)_6]^{3+}$ protons and uracil NH3 and guanine NH1 protons are well resolved. By recording a $[^1H,^1H]$-NOESY of the RNA in presence of $[Co(NH_3)_6]^{3+}$ in 90% H_2O / 10% D_2O, strong NOEs can be detected between the RNA and $[Co(NH_3)_6]^{3+}$ (Figure 7). This experiment naturally can only be successful, if $[Co(NH_3)_6]^{3+}$ is relatively tightly bound and no rapid dynamics occur.

Rüdisser and Tinoco have used this approach to position a $[Mg(H_2O)_6]^{2+}$ in their structure of a GAAA tetraloop [76]. They used distance constraints based on NOEs in the restricted molecular dynamics calculation. In order to calculate the geometry of the GAAA tetraloop-ligand complex, $[Co(NH_3)_6]^{3+}$ was placed randomly into the RNA starting structures with randomized torsion angles. Out of 17 converged structures, ten folded into geometries with $[Co(NH_3)_6]^{3+}$ in the major groove and seven structures had $[Co(NH_3)_6]^{3+}$ bound in the minor groove to the GAAA tetraloop. The predicted NOEs for the major groove binding mode were consistent with all experimental data, but the minor groove binding mode predicted NOEs that could not be seen. Therefore, the minor groove binding mode was excluded.

$[Co(NH_3)_6]^{3+}$ is considered a rather good mimic for fully hydrated $[Mg(H_2O)_6]^{2+}$ ions. However, it has to be kept in mind that $[Co(NH_3)_6]^{3+}$ is an exchange inert complex. Hence any Mg^{2+} binding site with more common partially dehydrated Mg^{2+}-acqua complexes will be missed.

3.2.2.4. *Inner-Sphere Coordination Detected by ^2J-[^1H,^{15}N]-HSQC*

The N7 of purine nucleotides is a well known metal ion binding site in nucleic acids [4,44]. One possibility to detect metal ion binding to this atom is the use of direct ^{15}N detection (see section 3.2.1.3). A big caveat of this method is the low ^{15}N gyromagnetic ratio leading to very weak signal and concomitantly high concentration requirements and prolonged recording times. To overcome these problems, we have recently used ^2J-[^1H,^{15}N]-HSQC experiments [80,81] that were optimized for the 11.4 Hz coupling between H8 and N7 of purine bases, to identify Mg^{2+} coordination to N7 of the 27 nucleotide long RNA hairpin D6-27 [82]. In this approach, either all adenosine or guanosine nucleotides are ^{13}C,^{15}N isotope labeled by *in vitro* transcription. Spectra are recorded upon addition of increasing concentrations of $MgCl_2$ and line-broadening effects as well as chemical shift changes are observed. In the case of D6-27, all monitored resonances show chemical shift changes in either the ^1H, the ^{15}N, or both dimensions. Some N7 chemical shifts experience line broadening and large upfield shifts, indicating direct coordination of a Mg^{2+} ion (Figure 8). Other resonances are "only" affected in their ^1H shift, being indicative of Mg^{2+}-induced local structural changes, but no direct binding. Due to the indirect detection of ^{15}N in the HSQC experiment, the signal intensity is comparable to the one of the directly observed ^1H. This renders the experiment much more sensitive than direct ^{15}N detection. Thus direct metal ion inner-sphere coordination to

N7 can be detected rapidly and extensive titration series can be performed without fear of sample degradation.

The corresponding experiment has recently been used to investigate the binding of Ag^+ to an imidazole modified DNA duplex, in which Ag^+ bridges two opposite imidazoles [61]. In this case, the ^{15}N resonances of the coordinating N3s are not only strongly upfield shifted but also split by 86 Hz due to the $^1J_{15N,107/109Ag}$ coupling with kinetically inert Ag^+ of spin ½ (see Section 3.2.1.3). It is well feasible that corresponding couplings are observable with ^{113}Cd in RNA, if the Cd^{2+} is tightly bound and experiences no exchange. Similar experiments have been performed with proteins in the past: M^{2+} binding to either N1 or N3 of histidine can be resolved by corresponding $^2J_{1H15N}$ experiments and in the case of cystein coordination, ^3J couplings can be observed in [$^1H,^{113}Cd$]-HMBC experiments [83-85].

3.2.3. *Direct Observation of Metal Ions*

Although the indirect methods of identifying metal ion binding sites via the classical "NMR-nuclei" ^1H, ^{15}N, ^{13}C or ^{31}P are generally robust, it would of course be preferable to obtain a NMR signature directly from the bound metal ions. Most metal ions that bind to nucleic acids possess significantly abundant, NMR active isotopes [86]. Unfortunately, most of them also have nuclear spin numbers of $I = 3/2$, 5/2 and 7/2 and thus suffer from fast quadrupole relaxation that broadens the NMR spectral lines.

In solid state NMR, line width broadening due to quadrupolar relaxation is less of a problem because of the absence of rapid reorientation [87]. This potential has been exploited in a number of studies using ^{23}Na, ^{25}Mg or ^{59}Co as NMR active nuclei [87-89].

On the other hand, also some successes have been reported using liquid state NMR. ^{25}Mg NMR was used in a line shape analysis together with atomic absorption spectroscopy to characterize weak magnesium binding sites on yeast tRNA^{Phe} [90]. Magnetic relaxation dispersion experiments were employed to detect ^{23}Na in the spine of hydration in the minor groove of B-DNA [91] and ^{205}Tl has been used as a K^+ mimic in the characterization of monovalent cation binding to a DNA G-quadruplex [92,93].

3.3. EPR and Related Methods

Electron paramagnetic resonance (EPR) spectroscopy is based on the analogous physical

concept as NMR, but employs the electron spin (instead of nuclear spin) of one or more unpaired electrons. Unpaired electrons are commonly introduced into RNA by attaching a spin-label, usually a stable nitroxide radical, at a specific location by site-directed spin-labeling (SDSL) [94]. Alternatively, also paramagnetic metal ions can be used, providing a direct handle to observe the environment of these ions within large biomolecular structures. EPR and related methods have been used in the past to investigate global folding and the dynamics, as well as to monitor metal ion binding to RNA. To look at global folding, two spin labels need to be placed at specific locations in an oligonucleotide by chemical methods [94]. Pulsed EPR techniques like pulsed electron-electron double resonance (PELDOR or DEER) [95,96] or more specialized ones like double quantum coherence (DQC-EPR) [97] are then applied to obtain accurate distances in the range from 1.5-8 nm. This application including a detailed methodical description has been excellently reviewed recently [98]. Dynamic features and interactions of biomolecules in the range from picoseconds to milliseconds can be measured by continuous-wave EPR (cw-EPR) and has been applied for example with the *Hammerhead* ribozyme [99]. This method has been thoroughly reviewed lately [94] and we encourage the reader to refer to this literature for more information and practical details.

In the following we will concentrate on the usage of EPR to monitor metal ion binding to RNA and provide a brief overview on the different EPR techniques applied. Again, this topic has recently been excellently reviewed including a detailed experimental description [100] to which we refer the more interested reader.

3.3.1. *Mn^{2+} as an EPR Probe for Metal Ions in RNA*

EPR has developed into a major method to investigate the interaction of paramagnetic ions to RNA. Mostly Mn^{2+} is used as a paramagnetic mimic for Mg^{2+}, but also other ions like Cu^{2+} [101] or the vanadyl ion [102] have been applied in the past. The physico-chemical properties of Mn^{2+} and its differences compared to Mg^{2+} have been summarized above in Section 2.2. Mn^{2+} has five unpaired electrons, is nearly always high spin, and usually displays an octahedral coordination sphere. A single isolated unpaired electron with spin $S = \frac{1}{2}$ gives rise to a single resonance in the EPR spectrum. High-spin Mn^{2+} with $S = 5/2$ shows six major lines that are separated by about 90 Gauss. However, these lines can be further split due to interactions with other electrons or nuclear

spins with I > 0. This spin-spin interaction is called hyperfine interaction and can occur either through-space (dipolar) or through-bond. Excluding additional second-order effects, the energy levels of the unpaired electrons are all split by the hyperfine-interaction with the nucleus of ^{55}Mn (I = 5/2) giving rise to theoretically 36 transitions. However, a significant degeneracy of the energy levels is true for most Mn^{2+} binding sites and thus only the six major lines are detected.

Upon coordination of Mn^{2+} to, e.g. RNA, the EPR properties change to allow examination of the binding site with respect to (i) a quantification of bound versus free Mn^{2+}, (ii) gain information on the binding site of the biomolecule, and (iii) the identification of the ligating atoms by more advanced methods [100]. Methods to investigate these three characteristics shall be briefly summarized below, whereas a detailed description of the methodical work is reviewed in ref [100].

3.3.2. Quantification of Bound Mn^{2+} by Room-Temperature EPR

Mn^{2+} concentrations in solution can be quantified based on the integral of the peaks or estimated based on the signal height. If recorded at room temperature, binding of Mn^{2+} to a large biomolecule leads to a significant broadening of the EPR lines. This effect is due to the change from a perfectly symmetrical $Mn(OH_2)_6^{2+}$ to a Mn^{2+} coordinated to one or more atoms of the RNA. This effect increases with the size of the biomolecule because of slow molecular tumbling and the consequently longer rotational correlation times of the bound ion. By this method, Mn^{2+} binding to tRNA [103], the P5abc subdomain of a group I intron [100] as well as the *Hammerhead* ribozyme [104,105] have been quantified.

Lowering the temperature below freezing point after addition of a cryoprotectant allows to detect the isolated EPR signal of the bound Mn^{2+}, if conditions have been chosen such that all Mn^{2+} ions are bound to the RNA. Although these changes are very subtle, they allow for a more detailed examination of the coordination sphere as has been shown in the case of the *Hammerhead* ribozyme [106].

3.3.3. Identification of Mn^{2+} Ligands by ENDOR Spectroscopy

It is possible to characterize the Mn^{2+} binding site in RNA by the additional detection of a signal from the nucleic acid. Relevant nuclei on the RNA are ^{31}P (I = ½), ^{14}N (I = 1), ^{1}H (I = ½), or specifically labeled sites of ^{15}N (I = ½) or ^{13}C (I = ½). The hyperfine interaction between unpaired

Mn^{2+} electrons and the nuclear spin of the surrounding atoms is based on distance, orbital overlap, and the nuclear properties and are generally too weak to be seen in standard EPR. However, by using advanced techniques like electron-nuclear double resonance spectroscopy (ENDOR), such hyperfine interactions with nuclei up to 7 Å away from the paramagnetic ion can be revealed. In ENDOR, generally a single position in the EPR spectrum is monitored [100]. The application of ENDOR has for example shown that Mn^{2+} coordinates in an innersphere fashion to the *Hammerhead* ribozyme [106]. Again, the application of ENDOR, both in a cw- or pulsed-EPR mode, is described in detail in ref [100].

3.3.4. *ESEEM Spectroscopy*

Electron-spin echo envelope modulation (ESEEM) is the method of choice to detect weak anisotropic hyperfine couplings. The amplitude of modulation for the hyperfine coupling depends on the number of nuclei and the relationship between the nuclear dependent frequencies [100]. In X-band spectrometers (microwave frequency of $\nu \approx 9.75$ GHz), ^{14}N coordinated to Mn^{2+} can be well observed, making ESEEM very useful to detect Mn^{2+}-purine coordination: In the *Hammerhead* ribozyme, Mn^{2+} coordination to adenine and guanine N7 sites has been detected by ESEEM [107-109]. If different types of nuclei are coordinated to Mn^{2+}, the resulting spectrum corresponds to the product of the individual spectra. Consequently the hydration level of Mn^{2+} bound to RNAs can be quantified [110]. For more detailed informations on ESEEM please refer to ref [100].

3.4. Lanthanide(III) Luminescence

Aside from their usage as hydrolytic cleaving (see Section 4.3.1) and chemical shift or line broadening reagents (see Section 3.2.2.2), Lanthanide(III) ion complexes are very good luminescence sensors for biological applications. These ions have long luminescence life times, are resistant to photobleaching and offer the possibility of using multiple emission bands for ratiometric sensing [111,112]. Luminescence lifetimes are strongly dependent on the solvation state of the Ln(III) ion including also the formation of hydroxo species, as has been shown in the pioneering work compiled by Baes and Messmer [113]. Therefore direct excitation photoluminescence studies can yield important information on the coordination sphere of these metal ions, mostly Tb(III) and Eu(III). This has been used by Uhlenbeck and coworkers to study the binding of these two ions to the Hammerhead ribozyme [114]. However, the obtained results of the recovered luminescence

lifetimes are often not easily interpreted and thus in recent years strong efforts have been made by Morrow and others to establish the basics before trying to understand larger nucleic acid systems [115,116].

Only few studies have thus dealt so-far with nucleotides and/or smaller RNAs. Measurements in H_2O and D_2O have shown that at least one water molecule is lost upon binding of the Lanthanide(III) ion to either GTP or RNA at slightly acidic or neutral pH [117]. Along the same line, Eu(III) binding to small RNA hairpins and a GAAA tetraloop has been investigated: The results indicate that Eu(III) looses more water molecules from its inner shell of hydration than Mg^{2+} as comparison with ITC experiments show [118-120]. Recently, Greenbaum and colleagues have used Förster resonance energy transfer (FRET) between Eu(III) ions and Cy3 to identify three site bound metal ions in the U2-U6 snRNA [121,122].

Taken together, Lanthanide(III) luminescence offers a great potential to yield detailed pictures about the stochiometry of metal ion binding to RNA as well as to gain information on the inner coordination sphere. However, first experiments have shown that the interpretation of the experimental data is often rather complex and one is thus only a the very beginning to really exploit this method.

3.5. Vibrational Spectroscopies

Vibrational spectroscopies have been commonly used as a standard technique to structurally characterize small molecules. The bond stretching, bending and deformation frequencies are strongly dependent on the nature of the atoms involved, the respective binding geometries, as well as their further bonded atoms. These vibrational modes become excited by electromagnetic radiation in the infrared range as long as a change in dipole moment is associated. To obtain an optimal signal-to-noise, mostly Fourier-transform infrared spectroscopy (FT-IR) is applied nowadays.

FT-IR is a well established method to investigate structural changes of proteins, DNA and RNA, i.e. conformational transitions upon ligand, drug, or protein/nucleic acid binding [123-125]. A more detailed description on experimental aspects has recently been published by Joly [123]. Also metal ion coordination is directly observable by a change in the energy of the associated vibrational modes. Nevertheless, only very few examples exist in the literature where metal ion

binding is investigated by FT-IR. Reasons being the dynamic nature of metal ion binding, the rather weak binding, as well as the small number of nucleic acid building blocks, making it very difficult to observe specific atoms within a large RNA. Some of these problems can be overcome by isotopic labeling, or by monitoring H/D exchange [124] but so far, mostly the coordination of kinetically inert ions like Pt^{2+} [126,127], or structural changes induced by metal ion (complexes), e.g., B- to Z-transitions of DNA, have been investigated [126,128]. Nevertheless, there are examples, where FT-IR was used to investigate the interaction of DNA and RNA with Ag^+ [129] and As_2O_3 [130].

Most of the vibrational bands that are not observable by IR, i.e. those that are not accompanied by a change in dipole moment, are Raman active. The Raman effect is based on the inelastic scattering of monochromatic light and used to study vibrational, rotational, and other low-frequency modes in a system. Raman has the advantage that a much smaller number of bands are observed and that water itself is Raman-silent. With respect to RNA, Raman has been used as an interesting alternative to study catalysis of the hairpin ribozyme [131]: Surface-enhanced Raman spectroscopy (SERS) is a powerful tool to detect trace amounts of RNA that are adsorbed on a metal surface. Upon cleavage the single stranded RNA product dissociates from the hairpin ribozyme and interacts with the surface of silver colloids and can be detected at biological concentration in real time [131].

Raman spectroscopy has been repeatedly used to investigate metal ion binding to the nucleic acid backbone phosphate oxygens. Metal ion interactions thereby lead to a change in energy of the bonds vibrations. In this way, the interaction of various metals like Mg^{2+}, Ca^{2+}, Sr^{2+}, Ba^{2+}, Mn^{2+}, Co^{2+}, Ni^{2+}, Cu^{2+}, Zn^{2+}, Pd^{2+}, and Cd^{2+} with DNA have been examined in a semiquantitative way [132-135]. More recently, inner-sphere coordination between Mg^{2+} and the backbone of the HDV ribozyme was detected using Raman crystallography [136]. In another study, Harris and coworkers used this method to distinguish between inner-sphere and outer-sphere interactions as well as electrostatic effects of metal ion binding. Whereas all three modes contribute to an attenuation of the Raman signal, only inner-sphere coordination leads to a frequency shift to higher wave numbers of the symmetric vibration of the non-bridging oxygen atoms $\nu_SPO_2^-$ [137]. The authors could show that the shift in $\nu_SPO_2^-$ is dependent on the metal ion identity and can also be used as a quantitative mean to characterize specific metal ion binding events.

Both, FT-IR and Raman spectroscopy have so-far been applied rather rarely to solve problems

associated with metal ion binding to nucleic acids. However, with the rapid technological advancements in the past years, it becomes clear that the power and possibilities of both methods have only been exploited marginally and one can thus expect exciting results in the future.

3.6. Further Spectroscopic Methods

Aside from the methods described in the above Sections, other methods usually more associated with proteins find application in the characterization of metal ion-nucleic acid interactions. X-rays for example can also be used for small angle X-ray scattering (SAXS), extended X-ray absorption fine structure (EXAFS), or X-ray absorption near-edge structure (XANES) spectroscopy as briefly summarized in the following paragraphs.

Small angle X-ray scattering yields information about folding/unfolding, aggregation, ligand binding, extended conformations, shape and assembly states of macromolecules [138-141].The resolution limit is with 10 Å rather low, but SAXS can be applied to macromolecules of literally any size. Often in combination with other techniques, a rather accurate picture of shape, flexibility and conformational changes dependent on cofactors can be obtained [138-141]. For example, SAXS has been used to investigate complete solution structures of the VS ribozyme in solution [142], to look at riboswitch conformations [143], to characterize conformational states of ribozymes [144], to follow folding in a time-resolved manner [145], or to investigate the effect of metal ions on the order of transition states of two group I intron ribozymes [146]. Woodson and Thirumalai could show that the *Azoarcus* group I intron folding is described by two components, whereas the *Tetrahymena* folding has at least one intermediate [146] (see also Chapter 7). They conclude that in the first case, tertiary contact formation occurs with charge neutralization of the backbone, whereas in the second case, additional counterions are needed.

XANES and EXAFS are two variations of X-ray absorption spectroscopy (XAS) that differ in the incident energy of the synchrotron radiation applied. A prerequisite for any of these methods is that a metal ion is tightly and specifically bound. Accordingly, XAS is regularly applied to metallo-proteins or small complexes [147,148]. XAS has recently been used to investigate a highly negatively charged polyoxometalate $[Mo_7O_{24}]^{6-}$ (POM) cluster hydrolyzing 2-hydroxypropyl-4-nitrophenyl phosphate as a RNA model substrate [149]. The investigators could show that the Mo(IV) in $[Mo_7O_{24}]^{6-}$ is actually the catalytically active species. Similarly it has been shown earlier

that a copper(III) hydroxysalen complex leads to site specific cleavage of the HIV-1 TAR RNA [150]. Very recently Fierke and colleagues have used XANES and EXAFS to look at metal ion binding in the P4 helix of RNase P [151]. The collected XAFS data show that a Zn^{2+} coordinates (at least) partly inner-sphere to the P4 helix in a octahedral coordination geometry with an average Zn(II)-O/N distance of 2.08 Å [151].

Another method yielding the corresponding information on local geometry is perturbed angular correlation (PAC) of gamma rays [152]. Certain radioactive nuclei decay by sending two gamma rays at a very short (10 nsec to 10 μsec) but defined interval at a specific angle to each other. The hyperfine interactions of the probe nucleus with the surrounding electric and/or magnetic fields allow to draw conclusions on the closer neighborhood. Originally a method to investigate solids, it has recently been applied to look at metal ion binding in proteins [147,148,153-156], using ^{111m}Cd and ^{199m}Hg. With respect to RNA, PAC is currently applied to investigate bridging Hg^{2+} ions between two uracil units forming U-Hg(II)-U base pairs in a RNA duplex [157].

To summarize, SAXS, XAS, and PAC are new methods that have rarely been applied yet, but with increasing understanding of metal ion interactions, will provide new ways to characterize in detail the coordination spheres and geometries of metal ions in nucleic acids.

4. CHEMICAL AND BIOCHEMICAL METHODS

Aside from spectroscopic methods described above in Section 3, (bio)chemical methods are frequently applied to gather information on metal ion binding, as well as elucidating their possible roles in ribozyme catalysis. All of these methods require either modification of the nucleic acid, the exchange of the *in vivo* cofactor by another metal ion and/or RNA cleavage. Nevertheless, crucial information is gained that could not be obtained by other methods.

4.1. Sulfur Rescue Experiments

In such assays, one or more specific oxygen atoms are probed for their importance in structure and/or catalysis of given RNA by replacing them with the larger and softer sulfur. Most often a non-bridging phosphate oxygen is probed [158,159], but also other positions like the 3' ribose oxygen or even a nucleobase oxygen have been replaced in the past [160]. Here we concentrate on the application of such experiments to detect metal ion binding: For example, if Mg^{2+} binding to a

specific phosphate oxygen is essential for catalysis, the activity of the ribozyme is reduced upon replacement with sulfur, due to the about two fold lower affinity of Mg^{2+} towards the softer sulfur ligand [161]. Upon addition of a more thiophilic metal ion like Cd^{2+} or Zn^{2+} [42,161,162] ribozyme activity may be restored [163]. Such a "rescue" is usually interpreted as evidence for inner-sphere metal-ion coordination to the phosphate oxygen.

In the following we will briefly summarize the incorporation of sulfur, the experimental setup, analysis and caveats of these experiments. For a detailed example the reader should also consider reference [26].

4.1.1. Incorporating the Phosphorothioate

Phosphorothioate nucleoside triphosphates (or phosphoamidites) containing a sulfur substitution at the position of one of the non-bridging oxygens of the α-phosphate are commercially available (e.g. from Glen research). They can be incorporated into the RNA either by *in vitro* transcription or by solid state synthesis. However, T7 RNA polymerase only accepts the S_P diastereomer of the phosphorothioate analog and incorporates it by inversion of configuration. This leads to RNA transcripts that carry only R_P phosphorothioates (see also Section 3.2.1.2) [164]. In addition the phosphorotioate nucleotide will be incorporated at every position complementary to the coding template strand.

In the case of solid state synthesis, both isomers are accepted and incorporated, leading to a mixture of R_P and S_P products. These can be separated by reverse phase HPLC, with the R_P derivative usually emerging prior to the S_P [55]. The identity of the stereoisomer can subsequently be tested by digestion with snake venom phosphodiesterase, which cleaves the S_P isomer more slowly than its R_P counterpart [165]. Unfortunately, chemical synthesis of RNA is restricted to about 70 nucleotides in length and the separation works well only for very small RNAs (up to 13 nt) [166]. Thus, one often depends on *in vitro* transcribed phosphorothioate RNA with the above mentioned caveats. Alternatively, if the modification is required near the end of a long strand, ligating a synthetically produced, modified oligonucleotide to a larger *in vitro* transcript may be an option [166]. In double stranded regions, simple annealing of a modified oligonucleotide may also work as it has been shown with other single atom modifications within the 23s ribosomal subunit [167].

4.1.2. Experimental Conditions

Sulfur rescue experiments have been widely used to identify metal ion binding sites in ribozymes and spliceosomal RNA [168-171]. A comprehensive review of the method is given in [26].

Most importantly, to determine the contribution of a specific metal ion to catalysis of a given ribozyme, it is imperative that the catalytic step is rate limiting. Therefore one generally uses single turnover conditions, in which the ribozyme is in large excess over the substrate. The 5' ^{32}P-labelled substrate is cleaved by addition of the either the wildtype or the sulfur substituted ribozyme in presence of Mg^{2+} or a thiophilic metal ion (e.g. Cd^{2+} or Zn^{2+}), respectively. Aliquots of the reaction solution are taken at different time points, quenched with EDTA, and all samples are then loaded on a denaturing polyacrylamide gel and analyzed by autoradiography.

Thiophilic metal ions often form insoluble metal oxide or hydroxide species at physiological pH. Hence, stock solutions of such metal ions are usually kept at acidic pH. Dilutions are best prepared freshly immediately prior to use. The pH of the final solution needs to be adjusted to fit the reaction conditions [166]. Elevated levels of monovalent salts are often used, both to saturate diffuse metal ion binding sites as well as to dampen indirect effects due to changes in ionic strength upon addition of thiophilic metal ions [166].

4.1.3. Data analysis

The intensity of the cleavage bands can be analyzed using, e.g., the ImageQuant software. For each experiment conducted either in the presence of Mg^{2+} and/or a thiophilic metal ion, the changing intensities are plotted versus time and fit to the appropriate kinetic equation [166]. To obtain a reliable fit, enough time points are required to give a non-linear least squares fit with $R^2 > 0.98$. As a rule of thumb, this requires usually about 10 data points, but optimization is required for each individual experiment.

To distinguish true thiophilic metal ion rescue from other effects, it is necessary to investigate both the modified and the unmodified RNA in presence and absence of the thiophilic metal ion. The relative rate of rescue (k_{rel}) can then be determined applying equation 1. This equation describes the rate enhancement of the phosphorothioate modified RNA with the thiophilic metal ion (k_S^M) over the reaction in the presence of Mg^{2+} only (k_S^{Mg}) normalized to the rate enhancement observed for the

unmodified RNA ($\frac{k_O^M}{k_O^{Mg}}$) [26,166]:

$$k_{rel} = \frac{\dfrac{k_S^M}{k_S^{Mg}}}{\dfrac{k_O^M}{k_O^{Mg}}}$$
(1)

Metal ion rescue experiments have also been used to determine the apparent affinity of a specific metal ion interaction by measuring the reaction rate over a range of metal ion concentrations [26].

4.1.4. Limitations

Although sulfur rescue experiments have been widely used to identify metal ion binding sites in ribozymes, the approach contains several pitfalls:

(i) First, it is usually assumed that the single atomic sulfur substitution does not perturb the structural integrity of the RNA. For many cases, this is true, but there are examples known where the presence of the larger sulfur disturbs the local structure [57,172]. Also from NAIM experiments (see Section 4.2.4) it is well known, that numerous phosphorothioate substitutions cannot be rescued [173]. Hence, the structural integrity has to be carefully confirmed before a sulfur rescue experiment is attempted.

(ii) Sulfur is simply different from oxygen: Aside from the ionic radius and electronegativity, these two elements also lead to different charge distributions (sulfur tends to make sigma bonds and hence forms no double bonds) in phosphorothioates and phosphates, and abilities to accept hydrogen bonds [26]. The larger diameter of the sulfur atom can also potentially impose steric constraints that impair the thiophilic metal ion from binding to the active site.

(iii) In case a rescue is observed, metal-ion thiophilicity alone cannot explain the efficiency of this process [174,175]. Whereas the Irving-Williams series of stability constants for metal-sulfur complexes follows the order $Cd^{2+} > Zn^{2+} > Ni^{2+} > Co^{2+} > Mn^{2+}$ [161,176,177] manganese is often the most efficient metal ion in thio-rescue experiments [26,173,174]. However, Mn^{2+} is not significantly more thiophilic than Mg^{2+}, but just has a slightly higher intrinsic affinity to both phosphates and thiophosphates [161,178]. A comparison of the basic affinities of various metal ions to phosphates and thiophosphate is given in Table 1 and Figure 2. Consequently other factors, such as the relative size, the preferred coordination geometry, and the hydration energy seem to be

critical in determining the ability of a certain metal ion to restore ribozyme activity. Especially the ionic radius of Cd^{2+} (1.03 Å) as compared to Mg^{2+} (0.86 Å) could be detrimental to phosphorothioate rescue because the original metal ion binding site has already been reduced in size by the bulky sulfur substituent [174]. At the same time it is also possible that the thiophilic metal ion binds to allosteric sites within the ribozyme and alters the rate limiting step of the reaction. It is therefore important to perform a rigorous thermodynamic and kinetic analysis of the reaction for all conditions, before conclusions are drawn from a sulfur rescue experiment [26].

Hence, although rescue of catalytic activity upon addition of a thiophilic metal ion to a sulfur substituted RNA is indicative for metal ion binding to this site, the opposite is not true: Lack of sulfur rescue does not proof that there is no metal ion binding site present. Rather, the experimental setup may not have been suitable to detect it.

4.2. Nucleotide Analogue Interference Mapping (NAIM)

In *Nucleotide Analog Interference Mapping* (NAIM), modified nucleotides are incorporated into the RNA by *in vitro* transcription as phosphorothioate nucleotide analogs. The pool of modified RNAs is then subjected to a stringent selection step (folding or catalysis), where active and inactive RNAs are separated. By iodine cleavage of the phosphorothioate linkage, modifications in each pool can be mapped. NAIM is a very elegant technique that allows the simultaneous characterization of chemical groups that are important for RNA function. For comprehensive protocols, we refer to ref [179] and [180]. Here, we just give a brief overview over the general method of NAIM and its applications for the identification of metal ion binding sites in RNA.

4.2.1. Methodology

NAIM consists of three distinct steps (Figure 9):

1. First, a pool of RNAs that contains phosphorothioate nucleotide analogs at random positions throughout the molecule is obtained by *in vitro* transcription. Subsequently, the RNAs are 5'- or 3'- end labeled with radioactive ^{32}P to allow detection by autoradiography.

2. In a second step, the RNA pool is subjected to a stringent selection, to identify chemical groups that are essential for RNA function. The active and inactive populations are separated by chromatography or native gel electrophoresis.

3. In the last step the positions of interference have to be mapped. This is done by iodine

cleaveage of the phosphorothioate bond and subsequent resolution of the cleaved positions on a

denaturing polyacrylamide gel and visualization by phosphor-imaging.

Some key points about the three steps are explained in more detail below:

Step 1 – Transcription and labeling: As discussed above in Sections 3.2.1.2 and 4.1.1, *in vitro* transcription by T7 RNA polymerase [10,164] leads to oligonucleotides that contain only R_P phosphorothioates. The ratio of unmodified and modified NTPs during transcription determines the incorporation level of the phosphorothioate tag and should be adjusted to about 5% [179]. Commercially available nucleotide analogs are usually sold at the required concentration to yield the optimal incorporation level for NAIM. Otherwise, this ratio has to be carefully re-established for each new analog. To incorporate NTPs with modifications at the 2'-hydroxyl position of the sugar moiety, a T7 RNA polymerase Y639F mutant has been developed [181].

Step 2 – Selection: It is of utmost importance to carefully optimize this step to ensure the successful outcome of the experiment [179]. Therefore, a basic characterization of the RNA and the processes that are subject of the NAIM analysis are a prerequisite for the successful optimization of the selection step. Two types of selection systems have been used in the past: In the case of ribozymes, active and inactive molecules are separated based on their length difference upon either self-cleavage or ligation with a substrate [180]. If folding is the required trait, native gel electrophoresis, which separates molecules according to their overall shape, is the method of choice. It is important that the gel solution does not contain denaturants such as urea, and should be performed at low voltage at 4°C. The gel solution should contain all cations that are needed for folding in the appropriate concentrations [180]. Reaction conditions are chosen, such as to yield 20 – 40% of folded relative to non-folded RNA [179].

Step 3 – Interference Mapping: Positions of interference are mapped by subjecting the two separated RNA pools to iodine cleavage and subsequent resolution of the pieces on a denaturing polyacrylamide gel (Figure 9a). Iodine cleaves the phosphodiester linkage of phosphorothioates, without affecting any other bonds in the RNA (Figure 9b). It is important to load all samples on the same gel and include controls for background degradation. For large RNAs (>250nt), it is advisable to run long gels (90cm) in addition to the standard sequencing gels (45cm), to increase the resolution [179]. Also, certain regions of the RNA may be better resolved using a higher or lower percentage of acrylamide, and for optimal results, these parameters need to be adjusted for each

new RNA.

The sites of interference are identified by quantification of the band intensities on the gel. The interference value κ (equation 2) is defined according to Strobel and Cochrane [180] as

$$\kappa = NF \times \frac{(N\alpha S_{experiment} / \delta\alpha S_{experiment})}{(N\alpha S_{unselected} / \delta\alpha S_{unselected})} \quad (2)$$

with NαS being the parent phosphorothioate nucleotide, δαS the phosphorothioate tagged nucleotide analog, and NF the normalization factor used to account for differences between loading and extent of reaction between lanes (typically between 0.8 and 1.2). A κ value >2 usually defines a site of nucleotide analog interference, whereas a value <0.5 one of enhancement.

4.2.2. Controls

In order to distinguish NAIM effects from direct interference of the phosphorothioate tag, it is crucial to transcribe the same RNA also in the presence of αS-NTPs without any further modification and subject these molecules to the same procedure (NαS in the above equation). Also, RNAs that have not undergone a selection step should be added as controls to analyze the overall level of analog incorporation into the RNA. If the incorporation level is too high, the bands at the bottom of the gel will be much stronger than those at the top of the gel, as multiple iodine induced cleavages occur in each RNA [180]. Unselected and uncleaved control samples are added to check for background degradation.

4.2.3. Choice of the Nucleotide Analog

A wide variety of nucleotide analogs is available these days, many of which commercially, or they can be synthesized using published protocols ([179] and refs herein). Three groups of analogs exist: Those deleting a functional group, those adding a steric bulk to the functional group and those altering the chemical nature of a functional group. It is important to define, which particular biochemical property is going to be investigated and to take into account the available structural and biochemical information on the system, before choosing a particular analog.

4.2.4. NAIM to Identify Metal Ion Binding Sites

NAIM is a viable method to identify metal ion binding sites and has been exploited in a number of studies [182-185]. Metal ion binding to the N7 position has been probed by 7-deaza-αS

analogs, to the N6 amino group of adenosine by N6-methyl-A-αS, and to probe the amino group in guanosine, inosine was used [184]. Identification of guanosine-O6-carbonyl ligands for metal ions has been achieved with 6-thioguanosine phosphorothioate (s6GαS) [180]. A main problem with this method to identify metal ion binding atoms, is that each of the above modifications can lead to an interference even in the absence of any interaction with a metal ion as the steric and hydrogen bonding properties of the functional groups are severely altered. Hence, again great care has to be taken in interpreting these results.

4.2.5. *Limitations*

Obviously, NAIM only works, if the analog can be incorporated successfully into the RNA. Some analogs are very poor substrates for the RNA polymerase and thus incorporation efficiency is very low. It is important to optimize the ratio between non-modified and modified nucleotides for each analog. Furthermore, incorporation of certain analogs can result in severe inhibition of RNA function, making it impossible to perform the selection step. Another drawback is the possibility of interference by the phosphorothioate substitution itself (see also Section 4.1). Apparently, sometimes, the inclusion of Mn^{2+} or a thiophilic metal ion in the reaction buffer can help to decrease the phosphorothioate effect [180].

However, one of the most severe limitations with respect to metal ion binding remains the difficulty to unambiguously assign an interference to the disruption of a RNA metal-ion interaction, and not the primary effect of the atomic modification (see also Section 4.1). A rescue by a metal ion might not be due to a direct coordination to the introduced sulfur atom, but rather close-by, e.g. thus reinstalling the active local structure that has been disturbed by the sulfur. Generally, RNAs are very flexible and adaptable molecules that are active under many conditions (i.e. high M^+ concentrations replacing Mg^{2+}, etc). It is unclear if under such varying conditions different catalytic strategies are employed, hence the metal ion binding sites found in thiorescue and NAIM experiments may not necessarily be equal to the ones present under physiological conditions.

4.3. Hydrolytic Cleavage Experiments

The detection of metal ion binding sites within large RNAs poses an enormous challenge due to the sheer size of the system, but also because one needs to distinguish between the specifically and diffusely bound ions. The inherent instability of RNA provides a good tool for specific metal

ion binding site detection: Solvated, higher valent metal ions are partially deprotonated and can as such either directly attack the phosphodiester bridge or mediate hydrolysis of the backbone through 2'-OH activation. The resulting fragments can then be detected by gel electrophoresis and the cleavage sites located. As the Mg^{2+} driven hydrolysis of the backbone is usually rather slow, other ions like lanthanide(III) ions or Pb^{2+} are applied, as discussed in the following sections.

4.3.1. Lanthanide Cleavage

Lanthanide(III) ions are rather good mimics of alkaline earth metal ions, e.g. Tb^{3+} for Ca^{2+}, as has been shown for metal-proteins interactions [186-188]. Also in RNA, lanthanide(III) ions are believed to bind mostly to the same sites as Mg^{2+}, albeit with higher affinity, due to their higher charge. Some physico-chemical properties of lanthanide(III) ions are summarized in Table 2. The pK_a values of the Ln^{3+}-coordinated water molecules are much closer to physiological value than those coordinated to Mg^{2+} [113,189], and hence hydrolysis of the RNA backbone mediated by the $M(H_2O)_n(OH)^{2+}$ is accelerated around neutral pH [38,190-192]. Especially Tb^{3+}, as well as Eu^{3+} have been successfully used in the past to determine metal ion binding sites in complex three dimensional structures of RNAs [192,193]. A detailed protocol on this method using terbium(III) can be found in the Handbook of RNA Biochemistry [194]. Below, we thus only state the most important points.

In the case of lanthanide(III) mediated cleavage of the RNA, it is crucial to work with homogenous samples and carefully optimized reaction conditions for every new construct. Parameters that need to be optimized include (i) reaction temperature (0-45 °C), (ii) incubation time (0.5 – 4h), (iii) Ln^{3+} concentration, (iv) lanthanide(III) ion identity, and (v) Ln^{3+} : Mg^{2+} ratio. Furthermore, the pH needs to be kept below 7.5 (6.5-7.0 is ideal), as more basic conditions lead to the formation of insoluble lanthanide(III)hydroxo species. The total RNA cleavage should be smaller than 10% to ensure that each RNA undergoes only a single cleavage event. The cleavage products can then be separated by denaturing PAGE and the location of the cleavage identified by a concurrently run alkaline hydrolysis cleavage ladder and a RNase T1 digest.

To identify high affinity metal ion binding sites, a competition experiment with increasing Mg^{2+} concentrations is carried out. The intensity of a particular band should decrease if Mg^{2+} is binding at that position. It is possible that not all Mg^{2+} binding sites are detected in a particular

RNA, because Tb^{3+} needs to bind close in space to the 2'-OH that acts as a nucleophile in the cleavage reaction. Also sites that are very specific for a certain metal type may escape detection. Nonetheless, lanthanide(III) ion cleavage is a very powerful method to simultaneously identify several specific metal ion binding site within a RNA.

4.3.2. Pb^{2+} Cleavage as a Probe for Single Stranded RNA Regions

Historically, Pb^{2+} has been one of the first mimics to investigate Mg^{2+} in RNA [190,195,196]. Nowadays, Pb^{2+} induced RNA cleavage is most well known for the leadzyme, an *in vitro* selected ribozyme [29,30] (see also Section 3.1.3). The leadzyme is surprisingly selective for Pb^{2+}, cleaving at the 5'-end of an internal bulge structure, and cannot be replaced by any other metal ion as a cofactor for the reaction. The logarithm of the rate of cleavage increases linearly between pH 5.5 and 7.0, implicating a Pb^{2+} coordinated hydroxide as a general base [31].

Otherwise, highly specific Pb^{2+} cleavage is rarely observed. More often, cleavage by Pb^{2+} is relatively weak and usually comprises several consecutive phosphodiester bonds [197]. Predominant cleavage sites involve bulges, loops and other single stranded RNA regions and thus Pb^{2+} is commonly used as a probe for flexible parts within a given RNA [198]. Nevertheless, some sequence specific bias has been found [199]: In general, single stranded regions that undergo extensive stacking interactions, such as tetraloops, are resistant to cleavage by Pb^{2+}. Single nucleotide bulges are more susceptible if they are flanked by pyrimidines rather than purines, whereas multiple nucleotide bulges are relatively little protected by their flanking regions. These findings have promoted the use of Pb^{2+} cleavage to detect conformational changes in RNAs, e.g. upon increasing concentration of other divalent metal ions [197]. This method has been used even *in vivo* with *E.coli* cultures growing under different conditions [200].

The experimental conditions of Pb^{2+} cleavage assays are very similar to the ones carried out with lanthanide(III) ions (Section 4.3.1): ^{32}P-endlabeled RNA is first properly refolded by heating to 90 °C in a suitable buffer and subsequent slow cooling to room-temperature (see also Section 3.1.1). Cleavage is initiated by the addition of Pb(acetate)$_2$ (10 – 100 mM) and incubation at room temperature for 5 min. The reaction is stopped with EDTA and the samples are analyzed by denaturing PAGE alongside an RNase T1 and an alkaline cleavage ladder and subsequent autoradiography [197,198]. Lower concentrations of Pb(acetate)$_2$ (μM to low mM range) can be

used to probe high affinity metal ion binding sites [197]. As an indication that such strong and specific cleavage sites observed at low Pb^{2+} concentrations colocalize with a Mg^{2+} binding site, competition experiments can be performed with increasing concentrations of Mg^{2+}. If Mg^{2+} competes for binding, cleavage should be suppressed. This approach has been used to determine K_D values for Mg^{2+} binding in RNA [201,202] (see also Section 6.2). Nevertheless, results should be interpreted with care, as just the increasing ionic strengths might be the reason for a reduced Pb^{2+} induced cleavage.

4.3.3. In-Line Probing

In-line probing is a classical method to monitor changes in tertiary structure, relying on the natural instability of nonstructured RNA at elevated pH [203]: Positioning of the nucleophilic 2'-OH "in-line" with the 5'-O-leaving group (i.e. in a linear 180° angle typical for S_{N2} reactions) promotes transesterification of the respective bridging phosphodiester [204]. In a typical A-form helix, such an orientation is precluded, whereas more flexible single stranded RNAs are free to explore the full conformational space and invariably sample the reactive "in-line" positioning of the relevant atoms. *In-line probing* exploits this tendency for RNA to differentially degrade depending on its structure to probe for motifs within a larger RNA. Any structural change, be it induced by a metal ion or any ligand can thus be elucidated by *in line probing*.

A good protocol for *in-line probing* is given in ref. [203]. In short, ^{32}P endlabeled RNA is incubated together with a suitable ligand at room temperature for 40 h in buffered medium at pH 8.3 under general conditions that allow for proper folding to the native state. The reaction is quenched with EDTA and the sample is loaded immediately on a denaturing polyacrylamide gel, together with a variety of controls: RNAse T1, alkaline hydroxy ladder, a sample of undigested precursor RNA to check for sample integrity at the beginning, and a control *in line probing* reaction where no ligand was added. As is obvious from this protocol, *in-line probing* corresponds to the Ln^{3+} and Pb^{2+} induced cleavage described above in Sections 4.3.1 and 4.3.2, but using Mg^{2+} instead (hence the higher pH and much longer reaction time): generally Mg^{2+} is the cofactor that activates the 2'-OH, however, also experiments have been performed where, e.g., amine functional groups of ligands activate the 2'-OH [205].

The cleavage bands are examined for increasing or decreasing intensity as a function of ligand

concentration. To calculate the apparent K_D, at which the cleavage reaction is half maximal, the *fraction of RNA cleaved* according to equation 3 is plotted versus the logarithm of the ligand concentration:

$$FractionRNAcleaved = \frac{samplevalue - min.value}{max.value - min.value}$$

(3)

Max. and min. refer to the highest and lowest cleavage values measured for each analyzed band. Alternatively, if a known binding stochiometry is known, e.g. 1:1, a corresponding non-linear least-squares fit can be applied (see also Section 6).

It is generally rather difficult to draw any conclusions on the local structure: While a metal ion may stabilize a given motif and thus protect the RNA from degradation, it can also lock the RNA in a "in line" position and thus promote cleavage. It is therefore important to carefully analyze the results obtained from an *in-line probing* experiment and compare them to complementary structural informations of the system before drawing a definite conclusion.

4.3.4. Limitations and Caveats of Hydrolytic Cleavage Experiments

The hydrolytic cleavage experiments described above in Sections 4.3.1 to 4.3.3 have the great advantages of (i) being widely applicable to all different kinds of RNA, (ii) making even very large RNAs amenable to structural probing, (iii) yielding a large number of metal ion binding sites in a single experiment, and (iv) of being performed rather easily and fast by standard biochemical techniques [26,188]. In addition, by stepwise concentration increase of the hydrolytically active metal ion and plotting the intensity of cleavage versus the concentration, binding constants can be calculated [188]. If applied in higher concentrations, i.e. millimolar, such experiments can also be used to probe secondary structures, as single stranded regions and non-helical regions are more prone to cleavage: For example the binding of the 5'-exon to the exon binding sites 1 and 2 (EBS 1 and 2) of a group II intron can be followed by the disappearance of the Tb^{3+} induced cleavage in these regions [188,193].

However, this kind of experiments are by far not "fast-selling" and care has to be taken in several respects: (a) These assays will not yield all metal ion binding sites, as only those are detected that are in close proximity to the 2'-OH, or position a H_2O ideally for hydrolysis. Consequently, metal ions located in the major groove will not be detected. (b) Cleavage intensities do not necessarily correlate with binding affinities of the metal ion at a given site [188] because

cleavage efficiency is strongly dependent on the correct geometry for an in-line attack. (c) Competing the hydrolytic metal ion M^{n+} by increasing Mg^{2+} concentrations might not yield a correct picture of Mg^{2+} binding and affinity, because in general a higher ionic strength will reduce the binding affinity of a given metal ion. (d) Every metal ion has slightly different properties, like size, charge, pK_a, coordination number and preference for N/O ligands. Consequently, these ions will also bind not only slightly differently, but possibly also at different places. It has been noted with different RNAs, i.e. in tRNAPhe [190] and in two different group II introns [188,193,206], that depending on the metal ion applied, different cleavage sites occur. Hence, the picture obtained for, e.g., Tb^{3+} might not reflect the true binding sites of Mg^{2+}.

Taken together, hydrolytic cleavage assays can yield highly valuable information on metal ion binding and tertiary structure, but again have to be interpreted with care.

4.4. Fenton Cleavage to Probe Metal Ion Binding Sites

Hydrolytic cleavage of the RNA backbone can also be achieved by redox chemistry, making use of the well-known Fenton reaction [207]: Fe^{2+} reacts with H_2O_2 to yield short-lived, highly reactive hydroxyl radicals that cleave the RNA chain in close spatial proximity to the bound metal ion. In combination with RNA, the reaction is often catalytically applied, i.e. ascorbate is added to reduce the Fe^{3+} back to Fe^{2+}:

$$Fe^{2+} + H_2O_2 \longrightarrow Fe^{3+} + \cdot OH + OH^-$$
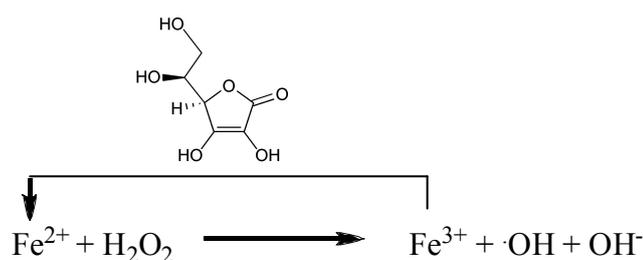
Classically, Fenton chemistry has been applied to probe for tertiary structures and mapping of binding sites of DNAs, proteins, RNA, and interactions thereof [208-214]: The relatively large $Fe(EDTA)^{2-}$ cannot penetrate a folded biomolecule and thus cleaves only the peripheral residues. Using Fenton chemistry it could be shown for the first time that RNAs other than tRNA and the ribosome are distinctly folded [215,216].

The Fenton reaction has also been exploited to characterize Mg^{2+} ion binding sites in RNA by using the just the solvated Fe^{2+}. Like Mg^{2+}, Fe^{2+} (and Fe^{3+}) possesses a predominantly octahedral

coordination geometry and can therefore replace the former in its binding pocket [217,218]. If Fe^{2+} is only applied in low micromolar concentrations in presence of sodium ascorbate [219], addition of H_2O_2 leads to the catalytic formation of hydroxyl radicals in close proximity to the Fe^{2+}/Fe^{3+} binding site. These radicals instantly cleave the RNA backbone and reveal the sites occupied by Fe^{2+}/Fe^{3+}.

Fenton cleavage is induced after proper folding of the ^{32}P-endlabeled RNA into its native structure by incubation in a buffer containing $0.2 - 20$ μM $Fe(NH_4)_2SO_4$ [220]. Incubation time and temperature need to be optimized for each RNA and vary between 5 and 30 min and 0 and 37 °C, respectively. The reaction is quenched by addition of loading buffer and the reaction products are separated by denaturing PAGE and analyzed by autoradiography. Care has to be taken to properly adjust the RNA:Fe^{2+} ratio for each individual case, because excessive free Fe^{2+} leads to unspecific RNA degradation [219]. Ideally the Fe^{2+} concentration is adjusted as to yield a single cleavage per molecule.

In general, the same limitations as for the other metal ion induced cleavage assays also apply here. If Fe^{2+} fails to substitute for a specific binding site of the native metal ion, this site will not be detected. On the other hand, false positives may occur due to the presence of alternative binding pockets for Fe^{2+}. A distinct difference to the hydrolytic cleavage described above in Section 4.3 is that hydroxyl radical cleavage is not limited to any geometry of the RNA binding site. Hence, $Fe^{2+/3+}$ specifically bound anywhere in the RNA, i.e. minor or major groove as well as loops, can be detected. In combination with, e.g. lanthanide(III) cleavage, an attribution to minor or major groove binding is feasible, but has to the best of our knowledge not yet been done.

5. COMPUTATIONAL METHODS

Especially for very large RNAs, the experimental methods are very limited if non-existent to identify metal ion binding sites or specify even single coordinating atoms. Hence, several *in silico* methods and databases have been developed in the past years to help overcome these deficiencies and to predict binding pockets for metal ions.

5.1. Theoretical Calculations

The negatively charged backbone of RNA molecules presents a large energetic barrier to

folding to complex structure. Thus cations, i.e. mostly metal ions, need to be involved, ranging in their binding behavior from a small number of specifically bound ions to a diffuse cloud of non-specifically bound ions. The latter is usually called an ion-atmosphere that surrounds any charged molecule in solution. Classically the role of metal ions in folding has been described by a simple Hill equation. However, physically, the Hill model can possibly not be correct: The overall charge of the system must equal zero, but a Hill fit to a folding transition yields a much lower number of metal ions than realistically needed. To overcome this obvious problem, Draper and colleagues have employed the non-linear Poisson Boltzman theory (NL-PB) to describe such an ion-atmosphere [35,221,222]. In the past years this theory has become widely used and found diverse applications in nucleic acids research (e.g. [35,223,224]). A typical outcome of such calculations is the electrostatic surface potential map that reveals regions of high negative charge potential that are likely to harbor metal ions (Figure 10) [225]. However, as with any model, there are limitations to the NL-PB theory, e.g., the solvent behaves like a simple continuum dielectric medium or solvated ions are point-like with no volume. Lately, one has begun to learn from experiments and to quantify the deficiencies in order to make better model systems. Such efforts have been excellently reviewed by Doniach and Herschlag [226] and shall thus not be explained in more detailed here.

An interesting possibility to scan for metal ion binding sites provides the web-based program FEATURE [227,228]: Originally developed to study the microenvironment of functional groups within proteins, it has now also been adapted to scan for metal ion binding sites within RNAs. Based on a set of known metal ion binding pockets and their microenvironment together with PB based electrostatic surface potential map, FEATURE scans RNA structures (i.e. the pdb file) of any size and predicts possible metal ion binding sites. In the case of a group I intron, known metal ion binding sites have thus been confirmed, whereas others were newly discovered, and can now be probed for by experimental techniques [228].

Highly sophisticated molecular modeling or quantum mechanics based methods to investigate the dynamics of RNAs and possibly catalytic mechanisms are still very rare. The pitfalls and advantages of these methods, especially QM/MM, which allows to investigate also larger systems, have recently been excellently reviewed [229,230] and shall thus not be described in more detail here.

In the following we will now concentrate on available databases that allow structural

characterization of metal ion binding pockets in nucleic acids.

5.2. Databases

To the best of our knowledge, three databases are available (all based on the PDB) that list RNAs and are specialized to investigate metal ion binding sites within. Each of these three databases has some special characteristics, which will be briefly described below. In addition, to these three databases, also a *Solvation Web Service* (SwS) for nucleic acids has been created by Auffinger and Hashem to provide an exhaustive overview of the solvation of nucleic acid [231].

5.2.1. Metalloprotein Database and Browser (MDB)

The Metalloprotein Database and Browser (MDB; http://metallo.scripps.edu) contains all metal ion-ligand interactions deposited within the PDB and NDB (Nucleic Acid Database) [232]. Its aim is to offer quantitative information on geometrical parameters of the primary metal ion coordination sphere. The database is searchable by different parameters like metal ion, number of ligands, R-value, resolution, author, or experimental technique. A Java applet allows then to visualize the metal ion together with its coordinating atoms.

5.2.2. MEtals in RNA (MeRNA)

The MeRNA database (http://merna.lbl.gov) compiles all metal ion binding sites identified in three dimensional structures of RNA available from the PDB and NDB [233]. The metal ion binding pockets are identified according to distances between the metal and the nearest atoms, be they from nucleotides, amino acids, water, or other molecules. Again, the database is searchable by specific parameters like PDB identifier, metal ion, method or distance from metal to any ligand. A specialty of the database is certainly the incorporated classification and listing of eight known metal ion binding motifs, namely the YG pair, sheared GA pairs, the Mg^{2+} clamp, the metal ion zipper, the loop E motif, the AA platform, tetrads, and the G-phosphate Mg^{2+} binding motif.

5.2.3. Metal Ions in Nucleic AcidS (MINAS)

The MINAS database (http://www.minas.uzh.ch) is not restricted to RNA, but also includes all DNA structures within the PDB and NDB. As of June 2010, 2079 structures are deposited and compiled in MINAS containing a total of 43757 metal ions. Out of these, 715 structures contain

RNA that bind 26893 Mg^{2+}. Like the MDB and MeRNA databases, also MINAS is searchable with regard to metal ion, PDB ID, experimental method and containing macromolecule (Figure 11).

In addition, several other special features are part of MINAS: MINAS allows to search for any specific combination of coordinating atoms, e.g., O1P, O2P, N7, O6, or H_2O, or just any atom of a nucleotide. One can thereby exploit the first as well as the second coordination sphere, i.e. inner-sphere and outer-sphere binding, and define inter- as well as intranucleotide binding patterns. The output file then lists all according occurrences in the databank. Searches can be personalized and be either downloaded or saved online to retrieve at a later time. The output file contains all relevant information, like metal ion, coordinating atoms, PDB ID, as well as a link to a small pdb file that contains the coordinates of the full binding pocket including the nearer surroundings (Figure 11). This extract of the original pdb file contains again all relevant headers and can be downloaded, allowing for a detailed characterization of each binding site.

To summarize, each of the three databases has a different focus, allowing researchers to choose according to their needs. Whereas the MDB concentrates on the geometry of the coordinating atoms, MeRNA allows to search for specific binding motifs. MINAS distinguishes between inner- and outer-sphere coordination and thus provides the most detailed, but also most complex picture of each binding site.

6. CALCULATION OF BINDING CONSTANTS

Compared to proteins, metal ion binding to RNA is often weak and dynamic in nature. Yet, metal ions play an important role in fine tuning the active fold and the catalytic activity of ribozymes [3,4,44,45,234]. Specific metal ion binding sites within one RNA molecule often display similar affinities (mostly with K_D values in the lower millimolar range), meaning that these sites are in direct competition with each other [13]. Consequently, not all metal ions present in the solution are available at each binding site. This notion has direct consequences on the procedures to calculate intrinsic affinity constants for each site. Developing reliable tools for the calculation of affinity constants for such simultaneous binding events is important in order to understand the exact roles that metal ions play in RNA structure and function.

6.1. ISTAR – Intrinsic STAbilities of RNA Metal Ion Complexes

[^{1}H]-NMR chemical shifts are strongly affected by metal ion binding, i.e. by the change in electrochemical environment, and have been used previously to calculate affinity constants. Usually this is done by plotting the chemical shift change in ppm versus the added [Mg^{2+}] and subsequently fitting these curves to a nonlinear least-squares regression for a 1:1 bimolecular association scheme [13,38,51,235]. Although yielding rough estimates of binding affinities, this method has two major caveats: (i) Chemical shift change data of exchangeable protons should not be used for calculation, as they are affected by several effects and thus do not follow a 1:1 binding behavior (Figure 12a). (ii) The Mg^{2+} bind simultaneously to the various sites, having the consequence that the total amount of Mg^{2+} in solution is not equal the one available for each site.

The first problem can be solved by using chemical shift change data of non-exchangeable protons or other nuclei, .e.g. ^{15}N or ^{13}C. To tackle the second issue, we have recently developed a procedure that simultaneously takes into account all binding sites within one RNA during the calculation procedure [13], as briefly discussed below:

First, one needs to define the number of specific binding sites within the RNA under investigation. To do this, chemical shift change data of as many protons as possible are evaluated and preliminary affinity constants calculated. As one metal ion will affect many protons in close neighborhood, these constants are grouped according to their strengths, i.e. usually up to 10 protons "define" one binding pocket. These binding pockets can be verified by analyzing the line-broadening induced by Mg^{2+}- and Mn^{2+} coordination (see also Sections 3.2.2.1 and 3.2.2.2). The individual log K_A values of the evaluated protons are then averaged to obtain one affinity constant log $K_{A,av}$ per binding site.

As explained above, the available Mg^{2+} concentration for each site does not equal the total [Mg^{2+}] in solution, if numerous binding sites are present. To take this into account, one needs to calculate the amount of bound Mg^{2+} at each specific binding site i at every data point of the concentration by using log $K_{A,av}$ and equation 4:

$$\left[Mg^{2+}\right]_{bound,i} = [RNA \cdot Mg^{2+}]_i =$$

$$\left[Mg^{2+}\right]_{bound,i} = \frac{\left(K_{Ai}\left[Mg^{2+}\right]_{tot} + K_{Ai}\left[RNA\right]_{tot} + 1\right) - \sqrt{\left(-\left(K_{Ai}\left[Mg^{2+}\right]_{tot} + K_{Ai}\left[RNA\right]_{tot} + 1\right)\right)^2 - 4K_{Ai}^2\left[Mg^{2+}\right]_{tot}\left[RNA\right]_{tot}}}{2K_{Ai}} \qquad (4)$$

It follows that the amount of Mg^{2+} available for binding at each specific site is given by the

total Mg^{2+} concentration minus the amount bound to all other sites (equation 5):

$$\left[Mg^{2+}\right]_{avail,i} = \left[Mg^{2+}\right]_{tot} - \sum\left[Mg^{2+}\right]_{bound,tot} + \left[Mg^{2+}\right]_{bound,i} \tag{5}$$

The chemical shift changes are then again plotted versus $[Mg^{2+}]_{avail,i}$ and the curves fitted to a 1:1 binding isotherm to yield a new estimate for binding constants of all protons at this site. Again the obtained affinity constants are averaged to yield a new log $K_{A,av}$ for each binding site (Figure 12b). This procedure is iteratively repeated, until the average affinity constant (log $K_{A,av}$) of each binding site does not change anymore within the error limits [13].

We have automated the iteration procedure using the Matlab Toolbox (Matlab R2006a, Matworks Inc.) in a calculation tool called ISTAR [236], which is available from the authors. As input the chemical shift values from NMR experiments for as many protons as possible of a titration series with the metal ion of choice are needed.

6.2. Indirect Calculation of K_A Values via Competition

As mentioned in Section 4.3, competition experiments can be used to calculate affinity constants of specific metal ions at their binding sites. Lanthanide(III) cleavage or sulfur rescue with, e.g., Cd^{2+}, will decrease at sites of Mg^{2+} coordination upon addition of increasing amounts of magnesium salts. The procedure shall here be briefly described [237]: First, one needs to calculate the Ln^{3+} affinity at each cleavage site by plotting the change in intensity versus the increasing Ln^{3+} concentration and fitting the data with a 1:1 binding model (unless there is no clear evidence for a cooperative behavior or the like). Note that the single fit to a 1:1 binding model is justified in this case, as the Ln^{3+} usually exceeds the RNA concentration by at least a factor of 1000. This experiment then needs to be repeated at different Mg^{2+} concentrations in order to obtain the affinities of the Ln^{3+} ion under the various conditions. Plotting the change of Ln^{3+} affinities in dependence on the Mg^{2+} concentration and fitting this data to equation 6

$$K_{app,Ln} = \frac{K_{Ln}}{1 + K_{Mg}[Mg]_t} \tag{6}$$

will yield the intrinsic affinities of the Mg^{2+} at the single sites. It should be noted that in order to obtain meaningful values, the ionic strength needs to be equal in all experiments, i.e. the M^+

concentration needs to be reduced while increasing the Mg^{2+} concentration.

A drawback of the method lies in the fact that one can only roughly place the metal ion binding pocket, as in most cases several nucleotides are cleaved. In addition, various parameters need to by carefully adjusted and tested to make sure that the RNA is correctly folded and ribozymes are catalytically active under all applied conditions. The biggest advantage of the method is that in theory there is no size limit and thus even very large RNAs can be investigated.

6.3. Measuring Magnesium(II) Binding Stoichiometries by Equilibrium Dialysis

To measure the total amount of Mg^{2+} bound to RNA, two methods have mainly been exploited: Gel filtration and equilibrium dialysis. Gel filtration has the disadvantage that even the smallest columns need a few minutes to run, during which time reequilibration between free and bound Mg^{2+} will take place. Centricon ultrafiltration devices that are used in "forced equilibrium dialysis" [238] lead to a much faster separation of free and bound metal ions and have therefore given the most consistent results. First, the sample is allowed to equilibrate with a given concentration of solvated $MgCl_2$. The half time for equilibration lies in the order of seconds for a micromolar K_D [238]. The best way to test for sufficient equilibration time is to demonstrate, that doubling or halving the incubation time does not alter the final result. Once equilibrium is reached, the sample is added to a prewashed ultrafiltration device and centrifuged at maximum speed until a small percentage of the total volume has flown through. The metal ion content of the separated samples are analyzed using one of a variety of different techniques. Apart from atomic absorption spectroscopy, fluorescence measurements are most commonly used for that purpose. A number of commercially available fluorophores change their fluorescence intensity upon binding to Mg^{2+} (e.g. from Molecular Probes (Invitrogen) or ISS. Because many of the traditional Mg^{2+} chemosensors also detect Ca^{2+}, finding selective Mg^{2+} sensors is still an active area of research [239,240]. Several Mg^{2+} concentrations encompassing the range used in the final experiment are measured first, in order to establish a standard curve. The Mg^{2+} concentrations in the separated samples is then measured and compared with the standard curve. To avoid interference, the RNA should be denatured by guanidine HCl before measuring the fluorescence intensity. This method provides a quick and easy way of measuring the stoichiometry of magnesium ions bound to RNA, but it is not capable of determining, where these binding sites are located [238].

7. CONCLUDING REMARKS AND FUTURE DIRECTIONS

The investigation of metal ion binding to RNAs and the detailed characterization of this interaction is a highly challenging but fascinating task. Many methods as described in this chapter have been developed and optimized in the past, each one tackling the problem from a different angle and thus yielding complementary information. Although we are far from understanding metal ion coordination to RNAs, in the past few years novel approaches have been introduced and an increasingly rapid development has started to take place. It has become obvious that metal ion interactions with nucleic acids cannot easily be categorized: the majority of metal ions surrounding nucleic acids are used for charge screening of the phosphate sugar backbone, but an estimated 10% of divalent metal ions are bound more specifically, taking over structural as well as catalytic roles. The differentiation and observation of these site specifically bound metal ions in the presence of a large excess of equal ions (i.e. millimolar concentrations) in solution presents a major difficulty. In addition, the different roles cannot be distinguished clearly from each other, because structure and function are tightly linked, and metal ions influence basic properties of nucleotides over a distance of up to 15 Å [44].

Furthermore there seems to be no consensus on how RNAs employ metal ions, especially with respect to folding, but also on how the nucleic acid reacts to changes in metal ion concentration. This is not only true for, e.g., different classes of ribozymes, but often also for two ribozymes of the same kind (but slightly different sequence) stemming from the same gene [241]. Consequently one has to be very careful to generalize any new findings as each new RNA may hold unexpected surprises.

In spite of these difficulties, the multitude of methods summarized in this chapter enable us to look at metal ion coordination to RNAs from the most different perspectives in a truly interdisciplinary nature. Their combination, together with a profound reflection on the different physico-chemical properties and vast accumulated knowledge on related interactions with the nucleotide building blocks, provides the tools to investigate the relationship between nucleic acids and metal ions on the atomic level. New methods will certainly arise in the near future, often transferred from metalloproteins or other disciplines. Key directions in this sense are investigations on the dynamics of the metal ion-RNA interaction and experiments on the single molecule level.

ACKNOWLEDGMENTS

ABBREVIATIONS

AMP^{2-}	adenosine 5'-monophosphate
$AMPS^{2-}$	adenosine 5'-α-thiomonophosphate
Cy3	"cyanine 3", a fluorescent dye
cw-EPR	continuous-wave electron paramagnetic resonance
DEER	pulsed electron-electron double resonance
DQC-EPR	double quantum coherence electron paramagnetic resonance
EDTA	ethylendiamminetetracetic acid
ENDOR	electron-nuclear double resonance spectroscopy
EPR	electron paramagnetic resonance
ESEEM	electron-spin echo envelope modulation
EXAFS	extended X-ray absorption fine structure
FT-IR	Fourier-transform infrared spectroscopy
I	ionic strength
I	nuclear spin
ISTAR	*I*ntrinsic *STA*bilities of *R*NA metal ion complexes
ITC	isothermal calorimetry
GTP	guanosine 5'-triphosphate
HDV	Hepatitis Delta virus (ribozyme)
HIV-1 TAR	human immunodeficiency virus 1 trans-activation response (element)
HPLC	high-performance liquid chromatography
HSQC	heteronuclear single-quantum coherence
K_a	acidity constant
K_A	affinity constant
K_D	dissociation constant
MDB	*M*etalloprotein *D*atabase and *B*rwoser
MERNA	*ME*tals in *R*NA database
MINAS	*M*etal *I*ons in *N*ucleic *A*cid*S* database

NAIM	Nucleotide Analog Interference Mapping
NDB	Nucleic Acid Database
NL-PB	non-linear Poisson-Boltzman
NOESY	nuclear Overhauser effect spectroscopy
NTP	nucleoside 5'-triphosphate
PAC	perturbed angular correlation (spectroscopy)
PAGE	polyacrylamide gel electrophoresis
PDB	protein databank
PELDOR	pulsed electron-electron double resonance
POM	polyoxometalate
QM/MM	quantum mechanical / molecular mechanical
RNase P	ribonuclease P
S	electron spin
SAXS	small angle X-ray scattering
SDSL	site-directed spin-labeling
SERS	surface-enhanced Raman spectroscopy
snRNA	small nuclear ribonucleic acid
SwS	*Solvation Web Service*
TRIS	tris(hydroxymethyl)aminomethane
VS	Varkud satellite (ribozyme)
XAS	X-ray absorption spectroscopy
XANES	X-ray absorption near-edge structure

REFERENCES

1. J. L. Boots, M. D. Canny, E. Azimi and A. Pardi, *RNA*, 2008, **14**, 2212-2222.

2. M. Roychowdhury-Saha and D. H. Burke, *RNA*, 2006, **12**, 1846-1852.

3. J. Schnabl and R. K. O. Sigel, *Curr. Opin. Chem. Biol.*, 2010, **14**, 269-275.

4. E. Freisinger and R. K. O. Sigel, *Coord. Chem. Rev.*, 2007, **251**, 1834-1851.

5. R. K. O. Sigel and H. Sigel, *Acc. Chem. Res.*, 2010, **43**, 974-984.

6. M. C. Erat and R. K. O. Sigel, *J. Biol. Inorg. Chem.*, 2008, **13**, 1025-1036.

7. M. Steiner, D. Rueda and R. K. O. Sigel, *Angew. Chem., Int. Ed.*, 2009, **48**, 9739-9742.

8. K. Lang and R. Micura, *Nat. Protoc.*, 2008, **3**, 1457-1466.

9. C. Hoebartner, R. Rieder, C. Kreutz, B. Puffer, K. Lang, A. Polonskaia, A. Serganov and R. Micura, *J. Am. Chem. Soc.*, 2005, **127**, 12035-12045.

10. S. Gallo, M. Furler and R. K. O. Sigel, *CHIMIA*, 2005, **11**, 781-785.

11. B. Francois, A. Lescoute-Phillips, A. Werner and B. Masquida, in *Handbook of RNA Biochemistry*, ed. R. K. Hartmann, A. Bindereif, A. Schön, and E. Westhof, Wiley-VCH, Weinheim, 2008, Vol. 1, pp. 438 - 453.

12. M. C. Erat, in *Advances in Biomedical Spectroscopy*, ed. S. M. Pascal and A. Dingley, IOS Press, Amsterdam, The Netherlands, Vol. in press

13. M. C. Erat and R. K. O. Sigel, *Inorg. Chem.*, 2007, **46**, 11224-11234.

14. *NIST Critically Selected Stability Constants of Metal Complexes*, Reference Database 46, Version 6.4; data collected and selected by Smith, R. M. and Martell, A. E., U.S. Department of Commerce, National Institute of Standards and Technology, Gaithersburg, MD, U.S.A., 2001.

15. M. Furler, B. Knobloch and R. K. O. Sigel, *Inorg. Chim. Acta*, 2009, **362**, 771-776.

16. E. M. Bianchi, R. Griesser and H. Sigel, *Helv. Chim. Acta*, 2005, **88**, 406-425.

17. G. G. Liang, N. A. Corfu and H. Sigel, *Z. Naturforsch. B*, 1989, **44**, 538-542.

18. R. Tribolet, R. Malini-Balakrishnan and H. Sigel, *J. Chem. Soc., Dalton Trans., Inorg. Chem.*, 1985, 2291-2303.

19. H. Sigel and R. Griesser, *Chem. Soc. Rev.*, 2005, **34**, 875-900.

20.   B. E. Fischer, U. K. Häring, R. Tribolet and H. Sigel, *Eur. J. Biochem.*, 1979, **94**, 523-530.

21.   K. L. Buchmueller and K. M. Weeks, *Nucleic Acids Res.*, 2004, **32**, e184-.

22.   B. L. Golden and C. E. Kundrot, *J. Struct. Biol.*, 2003, **142**, 98-107.

23.   V. Tereshko, G. Minasov and M. Egli, *J. Am. Chem. Soc.*, 1999, **121**, 470-471.

24.   V. Tereshko, C. J. Wilds, G. Minasov, T. P. Prakash, M. A. Maier, A. Howard, Z. Wawrzak, M. Manoharan and M. Egli, *Nucleic Acids Res.*, 2001, **29**, 1208-1215.

25.   D. J. Klein, P. B. Moore and T. A. Steitz, *RNA*, 2004, **10**, 1366-1379.

26.   J. K. Frederiksen and J. A. Piccirilli, *Methods*, 2009, **49**, 148-166.

27.   H. W. Pley, K. M. Flaherty and D. B. McKay, *Nature*, 1994, **372**, 68-74.

28.   J. E. Wedekind and D. B. McKay, *Biochemistry*, 2003, **42**, 9554-9563.

29.   T. Pan and O. C. Uhlenbeck, *Biochemistry*, 1992, **31**, 3887-3895.

30.   T. Pan and O. C. Uhlenbeck, *Nature*, 1992, **358**, 560-563.

31.   T. Pan, B. Dichtl and O. C. Uhlenbeck, *Biochemistry*, 1994, **33**, 9561-9565.

32.   N. Sugimoto and T. Ohmichi, *FEBS Lett.*, 1996, **393**, 97-100.

33.   W. G. Scott, J. B. Murray, J. R. P. Arnold, B. L. Stoddard and A. Klug, *Science*, 1996, **274**, 2065-2069.

34.   W. Yang, J. Y. Lee and M. Nowotny, *Mol. Cell*, 2006, **22**, 5-13.

35.   D. E. Draper, D. Grilley and A. M. Soto, *Annu. Rev. Biophys. Biomol. Struct.*, 2005, **34**, 221-243.

36.   E. Ennifar, P. Walter and P. Dumas, *Nucleic Acids Res.*, 2003, **31**, 2671-2682.

37.   C. G. Hoogstraten, P. Legault and A. Pardi, *J. Mol. Biol.*, 1998, **284**, 337-350.

38.   R. K. O. Sigel, D. G. Sashital, D. L. Abramovitz, A. G. Palmer III, S. E. Butcher and A. M. Pyle, *Nat. Struct. Mol. Biol.*, 2004, **11**, 187-192.

39.   M. C. Erat, O. Zerbe, T. Fox and R. K. O. Sigel, *ChemBioChem*, 2007, **8**, 306 - 314.

40.   M. C. Erat, *Two Domains of Branching and Catalysis Act as Specific Metal Ion Binding Platforms Within the Group II Itron Ribozyme Core*, Ph.D. Thesis, University of Zürich, Zürich, 2007, pp. 348.

41.   I. Bertini and C. Luchinat, *NMR of Paramagnetic Molecules in Biological Systems*, Benjamin/Cummings, Menlo Park, CA, 1986.

42.   V. L. Pecoraro, J. D. Hermes and W. W. Cleland, *Biochemistry*, 1984, **23**, 5262-5271.

43. J. H. Davis, M. Tonelli, L. G. Scott, L. Jaeger, J. R. Williamson and S. E. Butcher, *J. Mol. Biol.*, 2005, **351**, 371-382.

44. R. K. O. Sigel and A. M. Pyle, *Chem. Rev.*, 2007, **107**, 97 - 113.

45. V. J. DeRose, *Curr. Opin. Struct. Biol.*, 2003, **13**, 317 - 324.

46. B. Knobloch, D. Suliga, A. Okruszek and R. K. O. Sigel, *Chem. Eur. J.*, 2005, **11**, 4163-4170.

47. M. K. Hansen, J.-P. Simorre, P. Hanson, V. Mokler, L. Bellon, L. Beigelman and A. Pardi, *RNA*, 1999, **5**, 1099-1104.

48. M. D. Tsai, in *Phosphorus-31 NMR: Principles and applications*, ed. D. Gorenstein, Academic Press, New York, 1984, pp. 175 - 196.

49. E. M. Osborne, W. L. Ward, M. Z. Ruehle and V. J. DeRose, *Biochemistry*, 2009, **48**, 10654-10664.

50. M. Maderia, L. M. Hunsicker and V. J. DeRose, *Biochemistry*, 2000, **39**, 12113-12120.

51. M. Maderia, T. E. Horton and V. J. DeRose, *Biochemistry*, 2000, **39**, 8193-8200.

52. R. B. Martin and Y. H. Mariam, *Met. Ions Biol. Syst.*, 1979, **8**, 57-124.

53. T. D. Son, M. Roux and M. Ellenberger, *Nucleic Acids Res.*, 1975, **2**, 1101-1110.

54. T.-D. Son and J. M. Neumann, *Nucleic Acids Res.*, 1977, **4**, 397-403.

55. G. Slim and M. J. Gait, *Nucleic Acids Res.*, 1991 **19**, 1183–1188.

56. E. Besic, *Investigation of the structural changes of the domain 6 of the group II intron ribozyme ai5γ due to metal ion binding at the branch-point.*, Master Thesis, University of Zürich, Zürich, 2007

57. K.-i. Suzumura, M. Warashina, K. Yoshinari, Y. Tanaka, T. Kuwabara, M. Orita and K. Taira, *FEBS Letters*, 2000, **473**, 106-112.

58. Y. Tanaka, C. Kojima, E. H. Morita, Y. Kasai, K. Yamasaki, A. Ono, M. Kainosho and K. Taira, *J. Am. Chem. Soc.*, 2002, **124**, 4595-4601.

59. Y. Tanaka and K. Taira, *Chem. Commun.*, 2005, **16**, 2069 - 2079.

60. Y. Tanaka and A. Ono, *Dalton Trans.*, 2008, 4965-4974.

61. S. Johannsen, N. Megger, D. Bohme, R. K. O. Sigel and J. Müller, *Nature Chem.*, 2010, **2**, 229-234.

62. E. Kellenbach, B. A. Maler, K. R. Yamamoto, R. Boelens and R. Kaptein, *FEBS Letters*, 1991, **291**, 367-370.

63. C. Damblon, C. Prosperi, L.-Y. Lian, I. Barsukov, R. P. Soto, M. Galleni, J.-M. Frere and G. C. K. Roberts, *J. Am. Chem. Soc.*, 1999, **121**, 11575-11576.

64. G. Wang, B. L. Gaffney and R. A. Jones, *J. Am. Chem. Soc.*, 2004, **126**, 8908-8909.

65. V. Markowski, G. R. Sullivan and J. D. Roberts, *J. Am. Chem. Soc.*, 1977, **99**, 714-718.

66. C. Wang, H. Gao, B. L. Gaffney and R. A. Jones, *J. Am. Chem. Soc.*, 1991, **113**, 5486-5488.

67. G. Bowmaker, A. , R. Harris, K. , B. Assadollahzadeh, D. Apperley, C. , P. Hodgkinson and P. Amornsakchai, *Mag. Res. Chem.*, 2004, **42**, 819-826.

68. G. C. van Stein, G. van Koten, K. Vrieze, C. Brevard and A. L. Spek, *J. Am. Chem. Soc.* , 1984, **106**, 4486–4492.

69. K. Wüthrich, *NMR of Proteins and Nucleic Acids*, John Wiley & Sons, New York, 1986.

70. J. L. O'Rear, S. Wang, A. L. Feig, L. Beigelman, O. C. Uhlenbeck and D. Herschlag, *RNA*, 2001, **7**, 537-545.

71. E. P. Nikonowicz and J. S. Smith, *Phosphorus, Sulfur and Silicon and the Related Elements*, 1999, **144-146**, 305-308.

72. J. C. Markley, F. Godde and S. T. Sigurdsson, *Biochemistry*, 2001, **40**, 13849-13856.

73. J. H. Davis, T. R. Foster, M. Tonelli and S. E. Butcher, *RNA*, 2007, **13**.

74. F. H.-T. Allain and G. Varani, *Nucleic Acids Res.*, 1995, **23**, 341-350.

75. S. E. Butcher, F. H.-T. Allain and J. Feigon, *Biochemistry*, 2000, **39**, 2174-2182.

76. S. Rüdisser and I. Tinoco, Jr., *J. Mol. Biol.*, 2000, **295**, 1211-1223.

77. J. S. Kieft and I. Tinoco, Jr., *Structure*, 1997, **5**, 713-721.

78. R. L. Gonzalez, Jr. and I. Tinoco Jr., *J. Mol. Biol.*, 1999, **289**, 1267-1282.

79. G. Colmenarejo and I. Tinoco Jr., *J. Mol. Biol.*, 1999, **290**, 119-135.

80. A. G. Palmer III, J. Cavanagh, P. E. Wright and M. Rance, *J. Magn. Reson.*, 1991, **93**, 151-170.

81. J. Noeske, C. Richter, M. A. Grundl, H. R. Nasiri, H. Schwalbe and J. Wöhnert, *Proc. Natl. Acad. Sci. USA*, 2005, **102**, 1372-1377.

82. M. C. Erat, H. Kovacs and R. K. O. Sigel, *J. Inorg. Biochem.*, 2010, **104**, 611-613.

83. E. A. Peroza, R. Schmucki, P. Guntert, E. Freisinger and O. Zerbe, *J. Mol. Biol.*, 2009, **387**, 207-218.

84. G. Digilio, C. Bracco, L. Vergani, M. Botta, D. Osella and A. Viarengo, *J. Biol. Inorg. Chem.*,

2009, **14**, 167-178.

85. K. Zangger, G. Oez, I. Armitage, M. and J. Otvos, D. , *Protein Sci.*, 1999, **8**, 2630-2638.

86. *NMR of Newly Accessible Nuclei:chemically and Biochemically important elements*, ed. P. Lazlo, Academic Press, New York, 1983.

87. C. V. Grant, V. Frydman, J. S. Harwood and L. Frydman, *J. Am. Chem. Soc.*, 2002, **124**, 4458-4462.

88. D. Rovnyak, M. Baldus, G. Wu, N. V. Hud, J. Feigon and R. G. Griffin, *J. Am. Chem. Soc.*, 2000, **122**, 11423-11429.

89. C. V. Grant, V. Frydman and L. Frydman, *J. Am. Chem. Soc.*, 2000, **122**, 11743-11744.

90. S. S. Reid and J. A. Cowan, *Biochemistry*, 1990, **29**, 6025 - 6032.

91. V. P. Denisov and B. Halle, *Proc. Natl. Acad. Sci. USA*, 2000, **97**, 629-633.

92. S. Basu, A. A. Szewczak, M. Cocco and S. A. Strobel, *J. Am. Chem. Soc.*, 2000, **122**, 3240-3241.

93. M. L. Gill, S. A. Strobel and J. P. Loria, *J. Am. Chem. Soc.*, 2005, **127**, 16723-16732.

94. X. Zhang, P. Cekan, S. T. Sigurdsson and P. Z. Qin, *Methods Enzymol.*, 2009, **469**, 303-328.

95. A. D. Milov, A. G. Maryasov and Y. D. Tsvetkov, *Appl. Magn. Res.*, 1998, **15**, 107-143.

96. M. Pannier, S. Veit, A. Godt, G. Jeschke and H. W. Spiess, *J. Magn. Res.*, 2000, **142**, 331-340.

97. P. P. Borbat, J. H. Davis, S. E. Butcher and J. H. Freed, *J. Am. Chem. Soc.*, 2004, **126**, 7746-7747.

98. O. Schiemann, *Methods Enzymol.*, 2009, **469**, 329-351.

99. T. E. Edwards and S. T. Sigurdsson, *Biochemistry*, 2005, **44**, 12870-12878.

100. L. Hunsicker-Wang, M. Vogt and V. J. DeRose, *Methods Enzymol.*, 2009, **468**, 335-367.

101. M. G. Santangelo, A. Medina-Molner, A. Schweiger, G. Mitrikas and B. Spingler, *J. Biol. Inorg. Chem.*, 2007, **12**, 767-775.

102. D. Mustafi, A. Bekesi, B. G. Vertessy and M. W. Makinen, *Proc. Natl. Acad. Sci. USA*, 2003, **100**, 5670-5675.

103. A. Danchin and M. Gueron, *Eur. J. Biochem.*, 1970, **16**, 532-536.

104. T. E. Horton, D. R. Clardy and V. J. DeRose, *Biochemistry*, 1998, **37**, 18094-18101.

105. N. Kisseleva, A. Khvorova, E. Westhof and O. Schiemann, *RNA*, 2005, **11**, 1-6.

106. S. R. Morrissey, T. E. Horton and V. J. DeRose, *J. Am. Chem. Soc.*, 2000, **122**, 3473-3481.

107. M. Vogt, S. Lahiri, C. G. Hoogstraten, R. D. Britt and V. J. DeRose, *J. Am. Chem. Soc.*, 2006, **128**, 16764-16770.

108. O. Schiemann, J. Fritscher, N. Kisseleva, S. T. Sigurdsson and T. F. Prisner, *ChemBioChem*, 2003, **4**, 1057-1065.

109. S. R. Morrissey, T. E. Horton, C. V. Grant, C. G. Hoogstraten, R. D. Britt and V. J. DeRose, *J. Am. Chem. Soc.*, 1999, **121**, 9215-9218.

110. C. G. Hoogstraten and R. D. Britt, *RNA*, 2002, **8**, 252-260.

111. W. D. Horrocks, Jr., *Methods Enzymol.*, 1993, **226**, 495-538.

112. R. M. Supkowski and W. D. Horrocks Jr., *Met. Ions. Biol. Syst.*, 2003, **40**, 281-322.

113. C. F. Baes, Jr. and R. E. Mesmer, *The Hydrolysis of Cations*, Krieger Publishing Co., Malabar, Florida, 1976, pp. 1-496.

114. A. L. Feig, M. Panek, W. D. Horrocks, Jr. and O. C. Uhlenbeck, *Chem. Biol.*, 1999, **6**, 801-810.

115. C. M. Andolina, R. A. Mathews and J. R. Morrow, *Helv. Chim. Acta*, 2009, **92**, 2330-2348.

116. I. Sanchez-Lombardo, C. M. Andolina, J. R. Morrow and A. K. Yatsimirsky, *Dalton Trans.*, 2010, **39**, 864-873.

117. D. Costa, M. L. Ramos, H. D. Burrows, M. J. Tapia and M. d. G. Miguel, *Chem. Phys.*, 2008, **352**, 241-248.

118. N. L. Greenbaum, C. Mundoma and D. R. Peterman, *Biochemistry*, 2001, **40**, 1124-1134.

119. C. Mundoma and N. L. Greenbaum, *J. Am. Chem. Soc.*, 2002, **124**, 3525-3532.

120. C. Mundoma and N. L. Greenbaum, *Biopolymers*, 2003, **69**, 100-109.

121. F. Yuan and N. L. Greenbaum, *Spectrum*, 2007, **20**, 14-17.

122. F. Yuan, L. Griffin, L. Phelps, V. Buschmann, K. Weston and N. L. Greenbaum, *Nucleic Acids Res.*, 2007, **35**, 2833-2845.

123. H. A. Tajmir-Riahi, C. N. N'Soukpoe-Kossi and D. Joly, *Spectroscopy*, 2009, **23**, 81-101.

124. A. Rodriguez-Casado, J. Bartolome, V. Carreno, M. Molina and P. Carmona, *Biophys. Chem.*, 2006, **124**, 73-79.

125. M. Banyay, J. Sandbrink, R. Stroemberg and A. Graeslund, *Biochem. Biophys. Res. Commun.*, 2004, **324**, 634-639.

126. T. Theophanides and H. A. Tajmir-Riahi, *J. Biomol. Struct. Dyn.*, 1985, **2**, 995-1004.

127. S. Nafisi and Z. Norouzi, *DNA Cell Biol.*, 2009, **28**, 469-477.

128. H. A. Tajmir-Riahi and T. Theophanides, *J. Biomol. Struct. Dyn.*, 1985, **3**, 537-542.

129. H. Arakawa, J. F. Neault and H. A. Tajmir-Riahi, *Biophys. J.*, 2001, **81**, 1580-1587.

130. S. Nafisi, A. Sobhanmanesh, K. Alimoghaddam, A. Ghavamzadeh and H.-A. Tajmir-Riahi, *DNA Cell Biol.*, 2005, **24**, 634-640.

131. A. Percot, S. Lecomte, J. Vergne and M.-C. Maurel, *Biopolymers*, 2009, **91**, 384-390.

132. J. G. Duguid, V. A. Bloomfield, J. M. Benevides and G. J. Thomas, *Biophys. J.*, 1993, **64**, A266-A266.

133. J. Duguid, V. A. Bloomfield, J. Benevides and G. J. Thomas, *Biophys. J.*, 1993, **65**, 1916-1928.

134. J. Stangret and R. Savoie, *Phys. Chem. Chem. Phys.*, 2002, **4**, 4770-4773.

135. M. Langlais, H. A. Tajmirriahi and R. Savoie, *Biopolymers*, 1990, **30**, 743-752.

136. B. Gong, Y. Chen, E. L. Christian, J. H. Chen, E. Chase, D. M. Chadalavada, R. Yajima, B. L. Golden, P. C. Bevilacqua and P. R. Carey, *J. Am. Chem. Soc.*, 2008, **130**, 9670-9672.

137. E. L. Christian, V. E. Anderson, P. R. Carey and M. E. Harris, *Biochemistry*, 2010, **49**, 2869-2879.

138. C. D. Putnam, M. Hammel, G. L. Hura and J. A. Tainer, *Quart. Rev. Biophys.*, 2007, **40**, 191-285.

139. J. Lipfert and S. Doniach, *Annu. Rev. Biophys. Biomol. Struct.*, 2007, **36**, 307-327.

140. R. P. Rambo and J. A. Tainer, *RNA*, 2010, **16**, 638-646.

141. R. P. Rambo and J. A. Tainer, *Curr. Opin. Struct.Biology*, 2010, **20**, 128-137.

142. J. Lipfert, J. Ouellet, D. G. Norman, S. Doniach and D. M. J. Lilley, *Structure*, 2008, **16**, 1357-1367.

143. J. Lipfert, D. Herschlag and S. Doniach, *Methods Mol. Biol.*, 2009, **540**, 141-159.

144. S. Doniach and J. Lipfert, *Methods Enzymol.*, 2009, **469**, 237-251.

145. L. Pollack and S. Doniach, *Methods Enzymol.*, 2009, **469**, 253-268.

146. S. Moghaddam, G. Caliskan, S. Chauhan, C. Hyeon, R. M. Briber, D. Thirumalai and S. A. Woodson, *J. Mol. Biol.*, 2009, **393**, 753-764.

147. U. Heinz, L. Hemmingsen, M. Kiefer and H.-W. Adolph, *Chem. Eur. J.*, 2009, **15**, 7350-

7358.

148. T. Liu, X. Chen, Z. Ma, J. Shokes, L. Hemmingsen, R. A. Scott and D. P. Giedroc, *Biochemistry*, 2008, **47**, 10564-10575.

149. G. Absillis, E. Cartuyvels, R. Van Deun and T. N. Parac-Vogt, *J. Am. Chem. Soc.*, 2008, **130**, 17400-17408.

150. C. Bailly, V. Guerniou, E. Lamour, J.-L. Bernier, F. Villain and H. Vezin, *ChemBioChem*, 2003, **4**, 112-114.

151. K. S. Koutmou, A. Casiano-Negroni, M. M. Getz, S. Pazicni, A. J. Andrews, J. E. Penner-Hahn, H. M. Al-Hashimi and C. A. Fierke, *Proc. Natl. Acad. Sci. USA*, 2010, **107**, 2479-2484, S2479/2471-S2479/2475.

152. L. Hemmingsen and T. Butz, in *Applications of Physical Methods to Inorganic and Bioinorganic Chemistry*, ed. R. A. Scott and C. M. Lukehart, John Wiley & Sons Ltd., Chichester, UK, 2007, pp. 423-439.

153. O. Iranzo, T. Jakusch, K.-H. Lee, L. Hemmingsen and V. L. Pecoraro, *Chem. Eur. J.*, 2009, **15**, 3761-3772.

154. O. Iranzo, P. W. Thulstrup, S.-b. Ryu, L. Hemmingsen and V. L. Pecoraro, *Chem. Eur. J.*, 2007, **13**, 9178-9190.

155. A. F. A. Peacock, L. Hemmingsen and V. L. Pecoraro, *Proc. Natl. Acad. Sci. USA*, 2008, **105**, 16566-16571.

156. N. Selevsek, S. Rival, A. Tholey, E. Heinzle, U. Heinz, L. Hemmingsen and H. W. Adolph, *J. Biol. Chem.*, 2009, **284**, 16419-16431.

157. S. Paulus, S. Johannsen, R. K. O. Sigel, P. W. Thulstrup and L. Hemmingsen, *to be submitted*.

158. S. C. Dahm and O. C. Uhlenbeck, *Biochemistry*, 1991, **30**, 9464-9469.

159. M. Forconi, J. Lee, J. K. Lee, J. A. Piccirilli and D. Herschlag, *Biochemistry*, 2008, **47**, 6883-6894.

160. P. M. Gordon, E. J. Sontheimer and J. A. Piccirilli, *RNA*, 2000, **6**, 199-205.

161. R. K. O. Sigel, B. Song and H. Sigel, *J. Am. Chem. Soc.*, 1997, **119**, 744-755.

162. C. P. Da Costa, A. Okruszek and H. Sigel, *ChemBioChem*, 2003, **4**, 593-602.

163. P. M. Gordon and J. A. Piccirilli, *Nat. Struct. Biol.*, 2001, **8**, 893-898.

164. A. D. Griffiths, B. V. Potter and I. C. Eperon, *Nucleic Acids Res.*, 1987. , **15**, 4145–4162.

165. P. M. Burgers and F. Eckstein, *Proc. Natl. Acad. Sci. USA*, 1978, **75**, 4798 - 4800.

166. E. L. Christian, in *Handbook of RNA Biochemistry*, ed. R. K. Hartmann, A. Bindereif, A. Schön, and E. Westhof, Wiley-VCH, Weinheim, 2008, Vol. 1, pp. 319 - 344.

167. K. Lang, M. Erlacher, D. N. Wilson, R. Micura and N. Polacek, *Chem. Biol.*, 2008, **15**, 485-492.

168. J. A. Piccirilli, J. S. Vyle, M. H. Caruthers and T. R. Cech, *Nature*, 1993, **361**, 85 - 88.

169. L. B. Weinstein, B. C. N. M. Jones, R. Cosstick and T. R. Cech, *Nature*, 1997, **388**, 805-808.

170. E. J. Sontheimer, S. Sun and J. A. Piccirilli, *Nature*, 1997, **388**, 801-805.

171. J. M. Warnecke, J. P. Fuerste, W. D. Hardt, V. A. Erdmann and R. K. Hartmann, *Proc. Natl. Acad. Sci. USA*, 1996, **93**, 8924-8928.

172. K. Kanaori, S. Sakamoto, H. Yoshida, P. Guga, W. Stec, K. Tajima and K. Makino, *Biochemistry*, 2004, **43**, 5672-5679.

173. M. Boudvillain and A. M. Pyle, *EMBO J.*, 1998, **17**, 7091-7104.

174. S. Basu and S. A. Strobel, *RNA*, 1999, **5**, 1399-1407.

175. C. A. Brautigam and T. A. Steitz, *J. Mol. Biol.*, 1998, **277**, 363-377.

176. H. Irving and R. J. P. Williams, *J. Chem. Soc.*, 1953, 3192-3210.

177. H. Sigel and D. B. McCormick, *Acc. Chem. Res.*, 1970, **3**, 201-208.

178. B. Knobloch, B. Nawrot, A. Okruszek and R. K. O. Sigel, *Chem. Eur. J.*, 2008, **14**, 3100-3109.

179. C. Waldsich, *Nature Protocols*, 2008, **3**, 811 - 823.

180. J. C. Cochrane and S. A. Strobel, *Curr. Protoc. Nucleic Acid Chem.* , 2004, Chapter 6: Unit 6.9.

181. R. Sousa and R. Padilla, *EMBO*, 1995, **14**, 4609 - 4621.

182. S. Basu, R. P. Rambo, J. Strauss-Soukup, J. H. Cate, A. R. Ferre-D'Amare, S. A. Strobel and J. A. Doudna, *Nat. Struct. Biol.*, 1998, **5**, 986-992.

183. S. Basu and S. A. Strobel, *Methods*, 2001, **23**, 264-275.

184. C. Waldsich and A. M. Pyle, *Nat. Struct. Mol. Biol.*, 2007, **14**, 37 - 44.

185. C. Waldsich and A. M. Pyle, *J. Mol. Biol.*, 2008, **375**, 572-580.

186. R. B. Martin and F. S. Richardson, *Quart. Rev. Biophys.*, 1979, **12**, 181-209.

187. *The Lanthanides and Their Interrelation with Biosystems*, ed. A. Sigel, H. Sigel, and R. K. O.

Sigel, Marcel Dekker Inc., New York, Basel, Hong Kong, 2003.

188. R. K. O. Sigel and A. M. Pyle, *Met. Ions Biol. Syst.*, 2003, **40**, 477-512.

189. S. Cotton, *Lanthanides and Actinides*, Macmillan Education Ltd., 1991.

190. J. Ciesiolka, T. Marciniec and W. J. Krzyzosiak, *Eur. J. Biochem.*, 1989, **182**, 445-450.

191. N. G. Walter, N. Yang and J. M. Burke, *J. Mol. Biol.*, 2000, **298**, 539-555.

192. S. Dorner and A. Barta, *Biol. Chem.*, 1999, **380**, 243-251.

193. R. K. O. Sigel, A. Vaidya and A. M. Pyle, *Nat. Struct. Biol.*, 2000, **7**, 1111-1116.

194. D. A. Harris and N. G. Walter, in *Handbook of RNA Biochemistry*, ed. R. K. Hartmann, A. Bindereif, A. Schön, and E. Westhof, Wiley-VCH, Weinheim, 2008, Vol. 1, pp. 205 - 213.

195. R. S. Brown, J. C. Dewan and A. Klug, *Biochemistry*, 1985, **24**, 4785-4801.

196. R. S. Brown, B. A. Hingerty, J. C. Dewan and A. Klug, *Nature*, 1983, **303**, 543-546.

197. L. A. Kirsebom and J. Ciesiolka, in *Handbook of RNA Biochemistry*, ed. R. K. Hartmann, A. Bindereif, A. Schön, and E. Westhof, Wiley-VCH, Weinheim, 2008, Vol. 1, pp. 214 - 227.

198. E. Huntzinger, M. Possedko, F. Winter, H. Moine, C. Ehresmann and P. Romby, in *Handbook of RNA Biochemistry*, ed. R. K. Hartmann, A. Bindereif, A. Schön, and E. Westhof, Wiley-VCH, Weinheim, 2008, Vol. 1, pp. 151 - 171.

199. J. Ciesiolka, D. Michalowski, J. Wrzesinski, J. Krajewski and W. J. Krzyzosiak, *J. Mol. Biol.*, 1998, **275**, 211-220.

200. M. Lindell, P. Romby and E. G. H. Wagner, *RNA*, 2002, **8**, 534-541.

201. D. Labuda, K. Nicoghosian and R. Cedergren, *J. Biol. Chem.*, 1985, **260**, 1103-1107.

202. M. Brannvall, N. E. Mikkelsen and L. A. Kirsebom, *Nucleic Acids Res.*, 2001, **29**, 1426-1432.

203. E. E. Regulski and R. R. Breaker, in *Post-Transcriptional Gene Regulation*, ed. J. Wilusz, Humana Press, Totowa, NJ, 2008, Vol. 419, pp. 53 - 67.

204. G. A. Soukup and R. R. Breaker, *RNA*, 1999, **5**, 1308-1325.

205. D. J. Earnshaw and M. J. Gait, *Nucleic Acids Res.*, 1998, **26**, 5551-5561.

206. M. Hertweck and M. W. Müller, *Eur. J. Biochem.*, 2001, **268**, 4610-4620.

207. H. J. H. Fenton, *Proc. Chem. Soc.*, 1893, **9**, 113.

208. A. Draganescu and T. D. Tullius, *Met. Ions Biol. Syst.*, 1996, **33**, 453-484.

209. A. Flaus, K. Luger, S. Tan and T. J. Richmond, *Proc. Natl. Acad. Sci. USA*, 1996, **93**, 1370-1375.

210. T. D. Tullius, *Free Radic. Res.*, 1991, **12-13**, 521-529.

211. T. D. Tullius, *Nature*, 1988, **332**, 663-664.

212. T. D. Tullius, *Comprehensive Supramolecular Chemistry*, 1996, **5**, 317-342.

213. W. J. Dixon, J. J. Hayes, J. R. Levin, M. F. Weidner, B. A. Dombroski and T. D. Tullius, *Methods Enzymol.*, 1991, **208**, 380-413.

214. T. D. Tullius, *Curr. Opin. Struct. Biol.*, 1991, **1**, 428-434.

215. D. W. Celander and T. R. Cech, *Science*, 1991, **251**, 401-407.

216. J. A. Latham and T. R. Cech, *Science*, 1989, **245**, 276-282.

217. C. Berens, B. Streicher, R. Schroeder and W. Hillen, 1998, **5**, 163-175.

218. I. Hoch, C. Berens, E. Westhof and R. Schroeder, *J. Mol. Biol.*, 1998, **282**, 557-569.

219. G. Bauer and C. Berens, in *Handbook of RNA Biochemistry*, ed. R. K. Hartmann, A. Bindereif, A. Schön, and E. Westhof, Wiley-VCH, Weinheim, 2008, Vol. 1, pp. 238 - 249.

220. Y.-G. Ren, N. Henriksson and A. Virtanen, in *Handbook of RNA Biochemistry*, ed. R. K. Hartmann, A. Bindereif, A. Schön, and E. Westhof, Wiley-VCH, Weinheim, 2008, Vol. 1, pp. 345 - 353.

221. V. K. Misra and D. E. Draper, *J. Mol. Biol.*, 2000, **299**, 813-825.

222. B. Honig and A. Nicholls, *Science*, 1995, **268**, 1144-1149.

223. N. Korolev, A. P. Lyubartsev and L. Nordenskiold, *J. Biomol. Struct. Dyn.*, 2002, **20**, 275-290.

224. I. A. Shkel and M. T. Record, *Biochemistry*, 2004, **43**, 7090-7101.

225. K. Chin, K. A. Sharp, B. Honig and A. M. Pyle, *Nat. Struct. Biol.*, 1999, **6**, 1055-1061.

226. V. B. Chu, Y. Bai, J. Lipfert, D. Herschlag and S. Doniach, *Curr. Opin. Chem. Biol.*, 2008, **12**, 619-625.

227. M. P. Liang, D. R. Banatao, T. E. Klein, D. L. Brutlag and R. B. Altman, *Nucleic Acids Res.*, 2003, **31**, 3324-3327.

228. D. R. Banatao, R. B. Altman and T. E. Klein, *Nucleic Acids Res.*, 2003, **31**, 4450-4460.

229. P. Banas, P. Jurecka, N. G. Walter, J. Sponer and M. Otyepka, *Methods*, 2009, **49**, 202-216.

230. M. A. Ditzler, M. Otyepka, J. Sponer and N. G. Walter, *Acc. Chem. Res.*, 2010, **43**, 40-47.

231. P. Auffinger and Y. Hashem, *Bioinformatics*, 2007, **23**, 1035-1037.

232. J. M. Castagnetto, S. W. Hennessy, V. A. Roberts, E. D. Getzoff, J. A. Tainer and M. E.

Pique, *Nucleic Acids Res.*, 2002, **30**, 379-382.

233. L. R. Stefan, R. Zhang, A. G. Levitan, D. K. Hendrix, S. E. Brenner and S. R. Holbrook, *Nucleic Acids Res.*, 2006, **34**, D131-D134.

234. A. M. Pyle, O. Fedorova and C. Waldsich, *Trends Biochem. Sci.*, 2007, **32**, 138-145.

235. R. L. Gonzalez, Jr. and I. Tinoco, Jr., *Methods Enzymol.*, 2001, **338**, 421-443.

236. M. C. Erat, J. Coles, C. Finazzo, B. Knobloch and R. K. O. Sigel, *manuscript in preparation*.

237. R. K. O. Sigel, *details to be published*.

238. A. J. Andrews and C. Fierke, in *Handbook of RNA Biochemistry*, ed. R. K. Hartmann, A. Bindereif, A. Schön, and E. Westhof, Wiley-VCH, Weinheim, 2008, Vol. 1, pp. 251 - 258.

239. Y. Liu, M. Han, H.-Y. Zhang, L.-X. Yang and W. Jiang, *Org. Lett.*, 2008, **10**, 2873-2876.

240. D. Ray and P. K. Bharadwaj, *Inorg. Chem.*, 2008, **47**, 2252-2254.

241. R. K. O. Sigel, *Eur. J. Inorg. Chem.*, 2005, **12**, 2281-2292.

242. R. D. Shannon, *Acta Crystallogr.*, 1976, **A32**, 751-767.

243. W. E. Morf and W. Simon, *Helv. Chim. Acta*, 1971, **54**, 794-810.

244. L. Helm and A. E. Merbach, *Coord. Chem. Rev.*, 1999, **187**, 151-181.

245. S. F. Lincoln, *Helv. Chim. Acta*, 2005, **88**, 523-545.

246. Y. Inada, A. M. Mohammed, H. H. Loeffler and S. Funahashi, *Helv. Chim. Acta*, 2005, **88**, 461-469.

247. H. Sigel, C. P. Da Costa and R. B. Martin, *Coord. Chem. Rev.*, 2001, **219-221**, 435-461.

248. C. P. Da Costa, D. Krajewska, A. Okruszek, W. J. Stec and H. Sigel, *J. Biol. Inorg. Chem.*, 2002, **7**, 405-415.

249. L. Helm and A. E. Merbach, *Chem. Rev.*, 2005, **105**, 1923-1959.

250. A. F. Holleman and E. Wiberg, *Lehrbuch der Anorganischen Chemie*, Walter de Gruyter, Berlin, New York, 1985, pp. 1265-1279.

251. D. Parker, R. S. Dickins, H. Puschmann, C. Crossland and J. A. K. Howard, *Chem. Rev.*, 2002, **102**, 1977-2010.

252. R. J. P. Williams and J. J. R. Fraústo da Silva, *The natural selection of the chemical elements*, Clarendon Press, Oxford, 1996, pp. 1-646.

253. M. C. Erat, E. Besic, M. Oberhuber and R. K. O. Sigel, *results to be published*.

TABLES

Table 1. Comparison of some physico-chemical properties of Mg^{2+}, Ca2+, Sr^{2+}, Ba^{2+}, Mn^{2+}, Co^{2+}, Ni^{2+}, Zn^{2+}, Cd^{2+}, and Pb^{2+} in aqueous solution. Given are the ionic radii and the preferred coordination number (CN) of the M^{2+} ions, the enthalpy of hydration (ΔH_{Hydr}), the acidity constant ($pK^H_{M(H_2O)_n}$) of a water molecule in the aqua complex, the ligand exchange rate from the first coordination sphere of the metal ion (k_{exch}), the logarithm of the affinity towards acetate (log K_O), the affinity towards NH_3 (log K_N), the affinity towards the phosphate group in AMP^{2-} (log $K_{AMP,op}$) and the thiophosphate group in $AMPS^{2-}$ (log $K_{AMPS,calc}$) as well as the change in affinity going from AMP^{2-} to $AMPS^{2-}$ ($\Delta log \Delta_{M(AMPS)}$) (see also Figure 2).

	Ca^{2+}	Sr^{2+}	Ba^{2+}	Mg^{2+}	Mn^{2+}	Co^{2+}	Ni^{2+}	Zn^{2+}	Cd^{2+}	Pb^{2+}	ref.
Ionic radius (Å)	1.00 (1.12)[a]	1.18 (1.26)[a]	1.35 (1.42)[a]	0.72	0.83[b]	(0.58)[c] 0.75[b]	(0.55)[c] 0.69	(0.60)[c] 0.74	0.95	1.19	[242]
CN	6 (8)[a]	6 (8)[a]	6 (8)[a]	6	6	4/6	4/5/6	4/6	6	6 (8)[a]	
Preferred ligands	O	O	O	O	O/N	O/N	O/N	O	N/O	O	
ΔH_{Hydr} (kJmol^{-1})	1570	1386	1290	1858	1762	(1708)[c]	(1758)[c]	(1691)[c]	1640	1432	[243]
	(1657)[a]	(1461)[a]	(1361)[a]			1888	1951	1871		(1524)[a]	
$pK^H_{M(H_2O)_n}$ (25°C)	12.85 ± 0.1	13.29 ± 0.1	13.47 ± 0.1	11.44 ± 0.1	10.59	9.8	9.86	8.96	10.2	7.8	[113]
k_{exch} (s^{-1})	≈ 5·10^8	≈ 8·10^8	≈ 3·10^9	6.7 · 10^5	2.1 · 10^7	3.2 · 10^6	3.2 · 10^4	4.1 · 10^8	6.8 · 10^8		[244-246]
log K_O	0.52 ± 0.05	0.45 ± 0.07	0.42 ± 0.06	0.49 ± 0.04	0.75 ± 0.11	0.83 ± 0.05	0.78 ± 0.06	0.88 ± 0.19	1.26 ± 0.07	2.08 ± 0.04	[187]
log K_N	0.1	−0.1	−0.2	0.22 ± 0.02	0.87	2.09	2.77 ± 0.03	2.32 ± 0.1	2.60 ± 0.08	1.3	[187]
log $K_{AMP,op}$	1.45 ± 0.05		1.16 ± 0.04	1.56 ± 0.03	2.16 ± 0.05	1.94 ± 0.06	1.94 ± 0.05	2.13 ± 0.06	2.44 ± 0.05	2.94 ± 0.08	[161,247]
log $K_{AMPS,calc}$	1.24 ± 0.08		0.97 ± 0.07	1.22 ± 0.06	1.96 ± 0.11	1.67 ± 0.12	1.74 ± 0.09	2.27 ± 0.20	4.32 ± 0.14	4.79 ± 0.15	[161,248]
$\Delta log \Delta_{M(AMPS)}$	−0.01 ± 0.10		−0.06 ± 0.08	−0.03 ± 0.07	0.16 ± 0.12	0.07 ± 0.14	0.16 ± 0.10	0.66 ± 0.21	2.37 ± 0.15	2.55 ± 0.13	[161,248]

[a] The numbers in brackets refer to CN = 8. [b] High-spin electron configuration. [c] The numbers in brackets refer to CN = 4 (tetrahedral).

Table 2. Comparison of some physico-chemical properties of the Lanthanide(III) ions including La^{3+}. Given are the ionic radii (R$_{M3+}$, Å) [242] for coordination 8 (top line) and 9 (2nd line), the preferred coordination number (CN) of the aquated M^{3+} ions [249], the enthalpy of hydration (Δ H$_{Hydr}$, kJmol^{-1}) [250], the mean distance between the metal ion (Å) and a coordinated water molecule in crystal structures of Ln(H$_2$O)$_9$$^{3+}$ ions [251], the acidity constant ($pK^H_{M(H_2O)_n}$, 25 °C) of a coordinated water molecule [113], the ligand exchange rate from the first coordination sphere of the metal ion (k_{exch}, s^{-1})[249], as well as the oxidation states in aqueous solution [250].

	La^{3+}	Ce^{3+}	Pr^{3+}	Nd^{3+}	Pm^{3+}	Sm^{3+}	Eu^{3+}	Gd^{3+}	Tb^{3+}	Dy^{3+}	Ho^{3+}	Er^{3+}	Tm^{3+}	Yb^{3+}	Lu^{3+}
R$_{M3+}$	1.160	1.143	1.126	1.109	1.093	1.079	1.066	1.053	1.040	1.3027	1.015	1.004	0.994	0.985	0.977
	1.216	1.196	1.179	1.163	1.144	1.132	1.120								
CN	9	9	9	9	8,9	8,9	8,9	8	8	8	8	8	8	8	8
Δ H$_{Hydr}$	3238	3370	3413	3442	3478	3515	3547	3571	3605	3637	3667	3691	3717	3739	3760
M···OH$_2$	2.539	2.587	2.500	2.494	-	2.435	2.444	2.439	2.371	2.434	2.404	2.340	2.315	2.391	2.323
$pK^H_{M(H_2O)_n}$	8.5	8.3	8.1	8.0		7.9	7.8	8.0	7.9	8.0	8.0	7.9	7.7	7.7	7.6
k_{exch}			>5·10^8	>4·10^8				8.3·10^8	5.6·10^8	4.3·10^8	2.1·10^8	1.3·10^8	0.9·10^8	0.5·10^8	
ox. states	3	3, 4	3	3	3	3	3	3	3	3	3	3	3	3	3

FIGURE LEGENDS

Figure 1. Periodic Table of the elements with the metal ions essential for most organisms colored in magenta [252]. Those elements commonly used in the different methods described here and/or found in the MINAS database are underlaid in light blue.

Figure 2. (a) Binding of divalent metal ions towards acetate ($\square$, log K_O) and NH_3 ($\circ$, log K_N) follows the Irving-Williams series. log$K$ values as given in Table 1 are depicted and are valid for 25°C and $I = 0.5$ M; regarding Fe^{2+} and Cu^{2+}, see ref [14]. (b) Affinities of divalent metal ions towards the 5'-terminal phosphate group of AMP^{2-} ($\blacksquare$, log $K_{AMP,op}$) do not follow the Irving-Williams series. The same trend is valid for binding towards the thiophosphate group of $AMPS^{2-}$ ($\bullet$, log $K_{AMPS,calc}$) except that Cd^{2+} and Pb^{2+} show extraordinarily high affinities. The intrinsic increase in affinity upon substitution of a terminal oxygen by a sulfur atom (Δlog $\Delta_{M(AMPS)}$) is also given ($\blacktriangle$).

Figure 3. Nucleation of crystal formation occurs in the labile zone, when the precipitant concentration reaches equilibrium. Due to subsequent depletion of the RNA concentration in solution, the system moves to the metastable zone where crystals can grow.

Figure 4. (a) Octahedral Mg^{2+} placed into the electron density map illustrating how Mg^{2+} can be identified in crystal structures of RNA and distinguished from, e.g. H_2O carrying the same number of electrons [25]. Reproduced with permission from the RNA Society. (b) Overlay of three crystal structures showing the coordination of Mg^{2+}, Ba^{2+} and Zn^{2+} in the HIV dimerisation initiation site. The three metal ions do not overlap completely, but exhibit slightly different coordination spheres. This panel has been prepared by PYMOL (W. L. DeLano, 2002, http://www.pymol.org) based on the PDB IDs 462D, 1Y6S and 1NCL.

Figure 5. [^{1}H]-NMR spectra of a group II intron 27 nucleotide hairpin (D6-27) without (blue) and in presence of 30 mM $MgCl_2$ (red). Shown are the imino proton resonances of uracil NH3 and guanine NH1. Upon addition of Mg^{2+}, chemical shift changes and line width broadening are observed. Resonances with the strongest effects are marked with asterisks.

Figure 6. [^{31}P]-NMR spectra of a group II intron 27 nucleotide hairpin (D6-27) where the nonbridging R_P oxygens of all five uracils residues present were replaced by sulfur. ^{31}P resonances of bridging phosphodiester groups are clustered around 0 ppm whereas those of thiophosphate groups appear well resolved at around 60 ppm (inset). The ^{31}P resonances of the 5'-terminal triphosphate chain (α-, β-, and γ-phosphates) appear in the negative chemical shift range [253].

Figure 7. [^{1}H,^{1}H]-NOESY of D6-27 in the presence of 2.5 mM Co(NH$_3$)$_6$$^{3+}$ in 90% H$_2$O / 10% D$_2$O. The resonance of the ammine protons of [Co(NH$_3$)$_6$]$^{3+}$ at 3.65 ppm is indicated by a blue dotted line. The imino protons of D6-27 that give the largest NOEs to [Co(NH$_3$)$_6$]$^{3+}$ are also indicated.

Figure 8. Section of a [^{1}H,^{15}N]-HSQC of D6-27, optimized for the ^2J-N7H8 coupling of purines (11.1 Hz for guanine and 11.4 Hz for adenine), showing crosspeaks between H8 and N7 of adenines. Chemical shift changes (as highlighted by arrows) in the nitrogen dimension upon addition of 0 – 2.5mM MgCl$_2$ indicate direct metal ion coordination to N7.

Figure 9. (a) The 3 steps of NAIM: First, the phosphorothioate analogue is introduced at random positions in the RNA. In the second step, a stringent selection is applied to be able to separate active from inactive (or folded from unfolded) molecules. After iodine cleavage of the diester bond at phosphorothioate positions, the effect of the substitution is mapped by polyacrylamide gel electrophoresis. Untreated RNA and a pool of RNA that has not been subjected to the selection process are included as controls. A missing band in the folded/active species signifies that incorporation of the nucleotide analog at this position interfered with function/folding. In contrast, stronger bands in the active/folded species mark positions where nucleotide analog incorporation is beneficial. (b) Putative mechanism of iodine cleavage of thioated phosphodiester bonds. Alternatively sulfur could also act as the leaving group.

Figure 10. Electrostatic surface potential map of D6-27 with (right) and without (left) the residues shown. The negatively charged regions are shown in red (–40 kTe), whereas the positively charged

ones in blue (10 kTe). The surface potential was calculated with QNIFFT [225] and visualized with PYMOL (W. L. DeLano, 2002, http://www.pymol.org) based on the PDB ID 2AHT [39].

Figure 11. Databank of Metal ions in Nucleic AcidS (MINAS; J. Schnabl, P. Suter, R. K. O. Sigel, 2010, http://www.minas.uzh.ch). (a) Top section of a typical output of MINAS after a search for Mg^{2+} ions bound to three phosphate oxygens in an inner-sphere fashion. (b) Detailed neighborhood of Mg(9010) in the PDB file 2NZ4 as provided by MINAS. (c) View of Mg(9016) in 2NZ4 as given in the mini PDB file provided by MINAS.

Figure 12. Calculation of affinity constants by using NMR. (a) Change in chemical shift of a guanosine N1H proton within D5 of the group II intron Sc.ai5γ upon titration with Mg^{2+}. The experimental data can clearly not be fitted to a 1:1 binding model (red line) [237]. (b) Correction of available Mg^{2+} for a given binding site and fit of the experimental data with a 1:1 binding model upon iterative calculation with ISTAR. The fit becomes better with every additional iteration round [13].